NASA

Technical Memorandum 85023

Saturn as a Radio Source

M. L. Kaiser, M. D. Desch, W. S. Kurth,
A. Lecacheux, F. Genova,
B. M. -Pedersen

MAY 1983

National Aeronautics and
Space Administration

Goddard Space Flight Center
Greenbelt, Maryland 20771

SATURN AS A RADIO SOURCE

M. L. Kaiser and M. D. Desch
Laboratory for Extraterrestrial Physics
NASA/Goddard Space Flight Center
Greenbelt, Maryland 20771

W. S. Kurth
Department of Physics and Astronomy
University of Iowa
Iowa City, Iowa 52242

A. Lecacheux, F. Genova and B. M. Pedersen
Observatoire de Paris
92190 Meudon, France

Abstract Saturn has three nonthermal components to its radio spectrum - Saturn kilometric radiation, narrowband noise and related continuum, and Saturn electrostatic discharges. All three components were discovered by the Voyager mission. In this review we discuss the observational features, the source locations and the emission theories of each component.

The Saturn kilometric radiation (SKR) beams the isotropic equivalent power of 50 gigawatts at maximum intensity. The radiation takes place in the frequency range from as low as 3 kHz to about 1200 kHz, with peak intensity near 200 kHz in the kilometer wavelength band. The emission generally is observed in storms that wax and wane on a time scale of hours, with considerable fine structure occurring at the tens of kHz and several seconds level. The storms appear to be made up of bands that drift both upward and downward in frequency. Often the emission appears in the form of arcs whose orientation in the frequency-time plane is a strong function of observer location. The intense storms of kilometer wavelength radiation display periodicities on several time scales. The most fundamental of these periodicities is the tendency for storms to recur on the average every 10h 39.4m, which is inferred to be the rotation period of Saturn's global magnetic field. Occasionally storms are also modulated at a period of about 66h, possibly due to the influence of the satellite Dione. Finally, a strong correlation exists between the solar wind and the intensity of Saturn's radio emission. This modulation induces a long-term periodicity in the radio output of about 25 days, consistent with the solar rotation period. Saturn's kilometric radio emission is strongly polarized and probably circular. Right-hand polarization (radio astronomical sense) is observed when the observations are made from above Saturn's northern hemisphere, and left-hand polarization is observed from above the southern hemisphere. These observations are interpreted in terms of radiation near the electron gyrofrequency escaping in the extraordinary mode from two source regions, one in the northern hemisphere and one in the southern hemisphere. Variations in the emission intensity and recurrence pattern observed from the inbound and outbound trajectories of the two Voyagers suggest that the footprints of these sources ar confined to small regions above the Saturnian auroral zones and near the noon meridian. In view of

the inferred source locations and of the direct correlation between the radio emission and the solar wind flux at Saturn, remote measurement of the radio intensity probably provides information on energy deposition rates through the dayside polar cusps and into the auroral zones.

In addition to this intense component of Saturn's magnetospheric radio spectrum, there are weak narrow-band tones that can be observed at very low frequencies (< 10 kHz) within Saturn's magnetosphere. These tones may be associated with plasma sheet gradients in Saturn's inner magnetosphere. Saturn is also the source of low-level continuum radiation at frequencies below the solar wind plasma frequency. This radiation is trapped in the low density cavity formed by the outer Saturnian magnetosphere in a manner similar to the trapped continuum radiation at Jupiter and the earth. These weaker narrowband and trapped continuum radiation components of the Saturn radio spectrum are thought to be analogous to terrestrial and Jovian emissions. These emissions are presumed to be generated in the left-hand ordinary sense via a mode conversion process from electrostatic Bernstein waves near the upper hybrid resonance frequency.

These two magnetospheric radio components are complemented by a third component, possibly arising from atmospheric lightning. This component, dubbed SED for Saturn Electrostatic Discharges, appeared as very brief, intense, broadband bursts that came in episodes separated by about 10h 10m, distinctly faster than the magnetospheric emission's repetition rate. Initial analysis suggested that the SED originated in the B-ring of Saturn where the Keplerian orbital period matches the observed periodicity. However, subsequent work showed that this was unlikely, and that SED are best explained as radio bursts from a 60°-wide lightning storm complex in Saturn's equatorial zone.

1.0 INTRODUCTION

The announcement by the Voyager Planetary Radio Astronomy (PRA) team (Kaiser et al., 1980) of the unequivocal detection of low-frequency non-thermal radio emission from Saturn brought to an end the two decades of frustration arising from the search for these emissions. Several researchers (Smith and Douglas, 1957 and 1959; Smith, 1959; Smith and Carr, 1959; Carr et al., 1961) reported bursts of possible Saturnian origin in the frequency range from 18 to 22 MHz, although all of these authors pointed out that the association with Saturn was by no means certain. Observations in the wavelength range from 1 mm to about 70 cm failed to detect synchrotron emission similar to that observed in Jupiter's radiation belts (see Newburn and Gulkis, 1973, and references therin). Subsequent in situ measurements of the magnetic field strength and the particle populations by the Pioneer 11 and Voyagers 1 and 2 indicate that Saturn's radiation belts should not be a source of synchrotron emission. In a widely referenced paper, Brown (1975) reported the possible detection of Saturn radio bursts near 1 MHz using the radio astronomy instrument onboard the earth orbiting IMP-6 spacecraft. However, Kaiser (1976) was unable to confirm Brown's findings using data from a similar radio astronomy instrument onboard the RAE-2 spacecraft in lunar orbit. No radio astronomy investigations were carried aboard the Pioneer 11 spacecraft, and so not until early 1980, when the Voyager-1 spacecraft had approached to within 3 AU was Saturn's true radio signature in the kilometer wavelength band actually revealed. The subsequent measurements of Saturn's varied radio spectrum by the PRA and Plasma Wave Science (PWS) instruments indicate that the radio bursts reported prior to 1980 were probably not associated with Saturn.

In this review, we will describe the observations from the Voyager PRA and PWS instruments. The PWS instrument overlaps the PRA frequency coverage at the low frequency extreme (< 60 kHz) and extends the Saturn observations down to about 10 Hz. We will at all times be describing freely propagating nonthermal electromagnetic emission, i.e. emission that, in principle,

could be detected from a fairly large distance from the planet (except for the case of the trapped continuum radiation which is freely propagating only within the confines of the magnetospheric cavity). The in situ waves or plasma waves are described elsewhere in this book (see chapters by Scarf et al., and Neubauer et al.). Also, thermal radiation from Saturn's atmosphere will not be described here; the reader is referred to the review by Newburn and Gulkis (1973). The description of the observations will be followed by a discussion of the analysis of these observations completed by May, 1983.

1.1 INSTRUMENTATION

Before reviewing the observations, we describe the PRA and PWS instruments and discuss the trajectories of the two Voyagers as they approached and then receded from Saturn. Both the PRA and the PWS instrument have been fully described elsewhere (Warwick et al., 1977; Scarf and Gurnett, 1977), so only those details of specific relevance to the Saturn observations will be described here.

Both instruments use the same pair of orthogonally mounted 10-m antennas with PRA using them as separate monopoles, and PWS as a balanced dipole of 7-m effective length. With this antenna system, the directivity at frequencies below a few MHz is very poor, so that direction-finding is purely inferential. The PRA instrument combines the signals from the monopoles in a 90° hybrid and measures incident radio wave power in the left hand (LH) and right hand (RH) circular or elliptical polarizations. The PWS instrument measures total received power in a given frequency band without reference to polarization.

The PRA instrument covers the frequency range from 40.5 MHz down to 1.2 kHz in two bands. The low frequency band covers the range from 1326.0 to 1.2 kHz in 70 1-kHz wide channels spaced 19.2 kHz apart. The high band covers the range from 40.5 to 1.5 MHz in 128 200-kHz wide channels spaced every 307.2 kHz. The sweep through the entire frequency range (both bands)

is accomplished in 6 seconds, with each individual channel requiring 25 msec of integration time plus 5 msec of settling time. The effective threshold of the instrument is limited by spacecraft generated noise and corresponds to an ability to detect a signal in the low band at 60 kHz of 3 x 10^{-20} W/m^2/Hz at 1 AU from the source. This detection capability improves by a factor of three above 150 kHz. However, the PRA high band suffers severely from spacecraft generated noise so that the detection capability is typically only 10^{-18} W/m^2/Hz at 10 MHz, which effectively limits observations to within a few hundred Saturn radii.

In the idealized case where the PRA monopoles may be considered as half dipoles, i.e. as monopoles erected above an infinite perfectly conducting plane, the responses of both antennas are elliptically polarized. Both polarization ellipses are identical in shape, having their major axes parallel to each other. The ellipticity varies with the source latitude above the plane of the monopoles. The polarization ellipses degenerate to a circle or a straight line when the radio source direction is respectively normal to or constrained in the plane of the monopoles. The indicated circular polarization degree, V_i, is obtained simply as the ratio of the difference to the sum of the detected power flux in each polarization channel. This quantity V_i and the received total power summarize the the information measured by the PRA instrument. V_i differs from the true circular polarization degree V (the fourth Stoke's parameter) by a proportionality coefficient which depends on the source latitude above the monopole plane and the 'cross-polarization' of the elliptical equivalent antennas. In addition, if the observed radiation contains a linearly polarized or unpolarized component, the antennas and wave polarization ellipses combine to give an over or under estimated degree of circular polarization, depending on whether the ellipse orientations differ by more or less than 45°. Within this ideal approximation and since the Saturn-spacecraft geometry is known, the polarization response of the PRA system could be determined unambiguously at each time. Unfortunately, the whole conducting structure of the Voyager spacecraft electrically interacts with the PRA monopoles and greatly complicates the interpretation of measurements of V_i. To date, only the sense of polarization, RH or LH, has been used in published analyses of Saturn's radio emissions.

The PWS instrument covers the frequency range from 10 Hz to 56.2 kHz in two different modes. In one mode, a 16 channel spectrum analyser is used. This spectrum analyser has four channels per decade sampled two channels at a time every 0.5 sec. The bandwidth is approximately 15% of the channel frequency. The PWS effective threshold at 50 kHz is about 10^{-18} $W/m^2/Hz$. The other PWS mode consists of an automatic gain control amplifier sampled 28800 times per second with 4-bit resolution which effectively provides a waveform analyser below 12 kHz.

1.2 THE VOYAGER TRAJECTORIES

Gurnett (1974) showed that a good coordinate system for organizing the earth's non-thermal radio emissions is the observer's magnetic latitude and solar hour angle (local time). This same coordinate system is also useful for Saturn (Warwick et al., 1981). For Saturn, the magnetic latitude is essentially the same as kronographic latitude because the Saturnian magnetic dipole moment is very nearly aligned with the rotation axis (see chapter by Connerney et al.).

Figure 1 shows the trajectories of both Voyager spacecraft projected onto the disk of Saturn. Here the solar hour angle is shown as local time with 12h corresponding to local noon, 24h local midnight, and 06h and 18h corresponding to the dawn and dusk meridians, respectively. For the months prior to closest approach to Saturn, both Voyagers were relatively fixed just north of the noon meridian in this coordinate system. Likewise, for the several month periods after the respective encounters, the Voyagers stayed relatively fixed with Voyager-1 at about 03.5h local time and $+26^{\circ}$ magnetic latitude, and Voyager-2 at 06h and -29° . Only during the few hours surrounding the closest approach times did the two spacecraft undergo significant movement in this coordinate system. For purposes of computing average properties of the Satrunian radio emission such as intensity and polarization, the reader should realize that less than 1/2 % of the unit sphere has been sampled. Contrast this with the earth (e.g. Gallagher and Gurnett, 1979) where spacecraft have observed the earth's radio emissions repeatedly from essentially all combinations of local time and magnetic latitude.

2.0 OBSERVABLE PROPERTIES

Saturn's nonthermal radio spectrum has three components, two of them originating in the magnetospheric plasma surrounding the planet, and the third most likely originating from lightning storms in the atmosphere. Table 1 compares the overall properties of these three components, and they are described in detail below.

2.1 MAGNETOSPHERIC RADIO EMISSIONS

Studies of the temporal, spectral and polarization behavior of Saturn's low frequency (< 1200 kHz) radio emission have substantially increased our understanding of the magnetospheric environment with which these emissions interact. To date, researchers have examined the emissions on time scales from fractions of a minute to months and have found that intensity modulations occur at or near periods of 10.66 hr, 66 hr, and 25 days. We will discuss the nature and modulation source of each of these periodicities. Additionally, non-periodic fluctuations have been observed and will be described.

Dynamic spectra of Saturn's kilometer wavelength emission clearly show several components. The first is a powerful wideband emission called Saturnian Kilometric Radiation (SKR) first described by Kaiser et al. (1980). It is observed sometimes as low as 3 kHz (Gurnett et al.,1981a) and as high as 1200 kHz (Warwick et al.,1981) with peak intensity at about 175 kHz. The other radio components overlap with SKR below 100 kHz, but have a different appearance including narrowband "tones", and a low-level "continuous" noise. These low frequency components are weak and sporadic, appearing only in the observations obtained near Saturn. They are described in section 2.1.3.

SKR was first observed in January, 1980 when the two spacecraft were at distances of >2 and >3 AU, respectively. Discrimination from Jovian emissions was made on the basis of polarization, spectral characteristics, and, most importantly, relative light travel time differences between the

two spacecraft. Figure 2 shows the discovery event. SKR appears as a patch of emission centered near 150 kHz, and persisting for about 1 hour. In this dynamic spectral display, the bottom panel of each pair shows total received power with increasing power indicated by increasing darkness. The top panel of each pair shows the sense of polarization of the received signal coded so that white corresponds to RH polarization, black to LH, and gray to unpolarized (or no emission). SKR appears as RH emission in this figure.

From a distance of 100 R_s (R_s = Saturn radius = 60330 km), Figure 3 shows a fairly typical 24 hour period of SKR with two episodes of emission, each lasting for several hours. These intervals of emission are made up of a number of discrete features such as narrowband drifting structures and brief intensifications. The overall pattern of the emission in the frequency-time plane is repetitive, but the individual features are not.

2.1.1 SKR modulations

Rotation --- One of the first recognized properties of SKR was the approximate 10.66 hour interval between major emission episodes (Kaiser et al., 1980). This result was somewhat surprising in view of the fact that the topology of Saturn's global magnetic field, as modeled by the Pioneer 11 investigators (Smith et al.,1980; Acuna and Ness, 1980), was such that no modulation of SKR was expected. That is, since Saturn's dipole field lacks any significant tilt relative to the spin axis and also is axisymmetric, no modulation due to a nodding motion of the radio beam or to magnetic anomaly-induced particle precipitation effects should occur. But observationally the spin modulation of SKR intensity (about 20 dB) is immediately evident. As viewed from some distance from the planet, the emission intensity waxes and wanes, disappearing for several hours then reappearing for several hours in episodes generally called radio storms. This can be seen in Figure 3, where the centers of the two episodes are about 11 hours apart. The recurrence period of storms can vary anywhere from about 9 to 13 hours, placing Saturn between earth and Jupiter in the degree to which it rotationally modulates its emission. Based on the central meridian longitude and the location of the satellite Io, Jovian

radio storms, for example, can be predicted to within ± several minutes at all frequencies, while the earth's auroral kilometer-wavelength emission (AKR) is only weakly modulated at a 24 hour period.

In spite of the modest rotation control that Saturn exercises, the planet's magnetic rotation period can be determined to within an uncertainty of several seconds if a long enough interval of time is analyzed. Implicit in this calculation is the assumption that the radio emission is tied to the planetary magnetic field which rotates rigidly with the planetary core. Using a 9-month-long (600-rotation) time series and applying a method of power spectral analysis, Desch and Kaiser (1981a) measured a period of 10h 39m 24s ± 7s, corresponding to a synodic rotation rate of 810.76 deg/day. Carr et al.(1981) also measured Saturn's period using SKR data and obtained a value 2 seconds shorter than that derived by Desch and Kaiser but statistically not inconsistent with it. Since this was the first measurement of Saturn's 'true', or magnetic, rotation period, and presumably that of its deep interior, Desch and Kaiser also described a coordinate system within which investigators might cast their results in a uniform and consistent fashion. They also provided an equation to transform from the old system used by Pioneer investigators to the new system. The new Saturn longitude system, usually referred to as SLS (1980), has its 0^{o} prime meridian facing Saturn's vernal equinox on Jan. 1.0, 1980. Like Jupiter's System III, it is a west longitude (left-hand) system; that is, longitudes at one point on the disk increase with time as viewed by a stationary observer.

The computation of SLS longitude proceeds in th following way: If t is the time of a given observation, t_o the system epoch (Jan 1.0 1980), D the observer-Saturn distance in km, and R the observer right ascension (angle in degrees in Saturn's equatorial plane from Saturn's vernal equinox to the observer), then the longitude, λ (SLS), of the meridian containing the observer is given by

$$\lambda \text{ (SLS)} = 810.76(t-t_o-D \times 3.86 \times 10^{-11})-R$$

The longitude is that facing the observer at the time the light or radio

signal left the planet. Note that since the rotation rate constant, 810.76, is in deg/day, $t-t_o$ must be expressed in days and fractions thereof. The rotation period of Desch and Kaiser and the coordinate system they proposed are now widely used by Saturn researchers.

Figure 4 shows histograms of the occurrence of SKR as a function of SLS. The top panel shows the SKR pattern observed before and after Voyager-1 closest approach as a function of the SLS of the spacecraft. The two histograms are of similar shape, but offset by more than 120°. Warwick et al. (1981) and Gurnett et al. (1981a) showed that this shift between the histograms was equal to the angle through which the Voyager-1 spacecraft moved during the encounter period (see Fig. 1). This was taken as direct evidence that the SKR radiation pattern is fixed relative to the sun, and does not rotate with the planet. This is shown more dramatically in the bottom panel of Figure 4 where the data from both pre and post encounter are displayed against sub-solar SLS. The two histograms of the top panel are merged into one with a strong peak in occurrence rate near 100° sub-solar SLS.

Since SKR is made up of discrete spectral components, it is difficult to determine the average spectral behavior. Carr et al. (1981) averaged long spans of pre encounter data containing both Saturn activity and inactive periods to produce longitude versus flux profiles at each PRA frequency channel, and an average flux versus frequency spectrum. Kaiser et al. (1980) showed SKR spectra in terms of the probability of detecting emission above a given threshold. Figure 5 shows the SKR spectra (normalized to an observer-Saturn distance of 1 AU) that are exceeded 50%, 10%, and 1% of the time. These observations were made by the Voyager-1 PRA instrument and are categorized into inbound and outbound spectra, corresponding to observations made from above the post-noon equator, and the post-midnight meridian, respectively (see Figure 1). Saturn appears to be a stronger radio source as observed from above its day side as compared to above the night side. The equivalent total isotropic radiated power is about 200 MW, 3 GW and 30 GW for the 50%, 10% and 1% occurrence levels inbound, respectively. The comparable values for the outbound observations are typically a factor of 3 to 4 less. Kaiser et al.(1981) pointed out that

this difference between inbound and outbound intensity levels is greatest at low frequencies. The flux density values are comparable at frequencies above 500 kHz, but differ by a factor of about 5 at 100 kHz.

Satellite control --- Long-term (periods>1 planetary rotation) modulations of the nonthermal radio emissions provide important evidence of phenomena occurring deep within the magnetosphere. Io modulation of the Jovian radio emission, for example, was the first indication of that satellite's particular astrophysical importance. Saturn's magnetosphere, like Jupiter's, contains satellites within a corotating magnetic field; however, Desch and Kaiser (1981b) reported no evidence of any persistent long-term modulation of SKR as might be revealed through power spectral analysis of long data spans. Near Voyager-1 Saturn encounter, however, Gurnett et al. (1981a) reported a short-lived modulation of SKR by Dione. SKR was observed to disappear every 66 hr, coincident with the period of revolution of Dione. The satellite phase at the time of the disappearances was about 270° (SLS). Desch and Kaiser (1981b) showed further that the modulation was strongly frequency dependent, being most pronunced at the lowest frequencies, that is below about 100 kHz, and not evident above about 250 kHz. This effect is shown in Figure 6, where we compare the power flux density spectrum of a normal, unmodulated SKR episode with an episode that displays apparent Dione control. Above about 80 kHz in this case, the two spectra have similar shapes, peaking at about 100 kHz and remaining relatively flat at higher frequencies. Below 80 kHz, however, the Dione-modulated emission falls off much more rapidly than does the normal spectrum, consistent with a strong low-frequency propagation effect, perhaps due to the presence of an intervening plasma of relatively high density. This idea was described by Kurth et al. (1981b) who attributed the refraction of SKR to the presence of a Dione-related plasma torus. According to this model, the longitudinal asymmetry is introduced by photosputtering off of localized bright features on the surface of Dione. Preferential sputtering would occur when the trailing hemisphere of the satellite is illuminated as is the case near 270° Dione phase.

Subsequent observations of putative Dione modulations have complicated this picture somewhat. Modulations near 66-hr period have also been

observed from days 337-349, 1980 by Voyager-1 (Desch and Kaiser, 1981b) and near Voyager-2 encounter on days 213-236, 1981 (Warwick et al., 1982). Moreover, the Voyager-2 observations showed an increase in SKR activity every 66 hours, rather than a decrease. Also, the phase of the later Voyager-1 and Voyager-2 modulations were 30° and 180°, respectively, not the 270° modulation phase of the earlier interval near Voyager-1 encounter. If these episodes were truly related to Dione, then the modulation is extremely complicated. All that can be said for certain at present is that the modulation at the Dione revolution period, which is strongly frequency dependent and phase variable, differs significantly from the way in which Io modulates the Jovian radio emission.

Solar wind control --- SKR is also observed to vary on a time scale of many days as was noted by Warwick et al. (1982) and Scarf et al. (1982). Sometimes this variation is quite dramatic as, for example, just after Voyager-2 Saturn encounter when SKR went completely undetected for 2-3 days after having appeared very strong just prior to and during encounter. At this time Voyager-2 was less than 0.04 AU from Saturn, so the detection threshold was about 4 orders of magnitude below nominal intensities at 200 kHz. These dropouts differ from the Dione- related modulations in that they generally last longer and occur over the entire ~1 MHz natural radiation bandwidth. Similar pronounced fluctuations have appeared in the SKR data extending back at least several months before both Voyager encounters.

In attempting to explain these dramatic variations in the SKR emission level, we note that several independent lines of evidence have suggested a strong solar wind influence at Saturn. For example, Bridge et al. (1982) tentatively invoked a plasma loss mechanism in Saturn's inner magnetosphere caused by a factor of two increase in solar wind pressure during the Voyager-2 flyby. Magnetic field observations (see chapters by Schardt et al. and Connerney et al.) motivated Behannon et al. (1981) and Ness et al. (1982) to attribute magnetic tail and magnetospheric size fluctuations to variations in the solar wind flux at Saturn. Finally, Warwick et al. (1982) and Scarf et al. (1982) hypothesized that the dramatic 2-3 day SKR disappearance described above might be due to the absence of solar wind flux at Saturn owing to the presence of the planet in Jupiter's magnetic

tail or tail filament (see e.g., Lepping et al. (1982) and Kurth et al. (1982b)). Kurth et al. (1982a) have shown evidence that Saturn may in fact have been immersed in Jupiter's tail at this time, based on the observation within Saturn's magnetosphere of Jovian-like low frequency continuum radiation.

Evidence of direct solar wind control of Saturn's radio emission was provided by Desch (1982). A typical example adapted from his study of how the radio emission level responds to solar wind conditions is shown in Figure 7. For example, a factor of 150 increase in solar wind pressure at Saturn and a 65% increase in bulk speed is accompanied by an order of magnitude increase in SKR emission level near June 5, 1981. A statistical analysis of two 160-day intervals of data yielded a significant correlation with ram pressure and a slightly lower overall correlation with bulk speed (Figure 8). In addition, just like the solar wind pressure, which exhibited a 25-day periodicity in magnitude over the extent of the analysis interval, SKR was also modulated in phase with the solar wind pressure at a period of 25 days. Since the location of the SKR source probably extends nearly to the cloud top or ionosphere level on Saturn (see section 3.1.1), the solar wind influence must also reach deep into the Saturnian magnetosphere.

In a recent continuation of this work, Desch and Rucker (1983) examined thirteen solar wind quantities and their relationship with SKR and showed that the solar wind ram pressure is the primary driver of Saturn's radio energy output. They view the results as consistent with the continuous mass transfer of particles from the solar wind into Saturn's low altitude cusp. This transport would proceed by means of eddy convection in the dayside polar cusp/magnetosheath region, as in a model developed for terrestrial magnetospheric processes (Haerendel et al., 1978).

Dynamic spectra variations -- Long-term modulations also appear in the shape of the dynamic spectrum itself, although apparently not with any well-defined periodicity. Figure 9 presents a compacted dynamic spectrum of Voyager-1 observations around encounter. The emission frequency range can be seen to vary considerably. In particular, the lowest frequency limit of the emission shifts from 20 kHz to more than 80-100kHz. These fluctuations

correspond to a distortion of the spectrum and not to a threshold effect due to temporary global intensity variations or change in distance. Genova et al.(1983) point out that this behavior is reminiscent of the earth's radio emission during magnetically quite times. They deduce that the changes in the SKR spectrum most likely reflect changes in the SKR source region, rather than, say, variable propagation effects.

2.1.2 Polarization of SKR

The interpretation of the recorded SKR polarization was simple and immediately suggested to Warwick et al. (1981,1982) the existence of two distinct radio sources, each emitting in the opposite sense of polarization and observed in various conditions of visibility by each spacecraft along its trajectory. This simple polarization behavior is quite different from that of the Jovian hectometer-wavelength emissions detected in the PRA low band, which showed frequent polarization reversals or events with mixed polarization (Alexander et al., 1981).

The SKR polarization behavior, in terms of the parameter V_i (see section 1.1), is shown in Figure 10 for several days around the planetary encounters. V_i indicates RH (LH) polarization sense when it is negative (positive). The polarization exhibits a nearly constant value, except during the close encounter periods or the spacecraft rolls, and is nearly independent of frequency. Along the pre encounter paths (see Figure 1), the recorded dynamic spectra appeared dominated by RH polarization, with only occasional periods of LH emission that are due to detections of the weaker LH polarized source. After the planetary fly-bys, Voyager-1 observed exclusively RH polarization, while Voyager-2 detected mostly LH emission. During the few hours around the Saturn closest approaches, the observations showed more complicated patterns, well in agreement with visibility changes from one polarization source in one hemisphere to the other, and with changes in the antenna-source geometry accompanying spacecraft rolls and motion along the fly-by trajectory (Warwick et al., 1981). Because the direction to the radio source is not in general normal to the PRA antenna plane, V_i does not reach ± 1.0. However, note that V_i reaches a value very close to unity during the second half of day 317 of 1980 (Voyager-1), when

the source was received approximately in the direction normal to the PRA monopoles. This implies either pure circular SKR polarization or elliptical SKR polarization with a substantial linear component remaining for hours in the antenna plane.

2.1.3 Fine structure

SKR dynamic spectral arcs --- In the SKR dynamic spectra, episodes of very bursty emission are observed with time and frequency scales less than 48 sec and about 50-100 kHz, producing patchy patterns in dynamic spectra, as seen for instance in Figure 3 and Figure 11b. These impulsive bursts have not been studied in any detail, so it is not known if they form a recognizable category in SKR phenomenology. However, at least one sub structure in the SKR dynamic spectra has been studied, and that is the arcs described by Boischot et al. (1981) and Thieman and Goldstein (1981).

Figure 11 shows examples of the two kinds of arcs: Vertex Early (hereafter VE) and Vertex Late (VL) arcs (i.e. arcs appearing respectively as opening and closing parentheses). The amplitude of the modulation of the arc emission is only a few decibels on average. The frequency extension of the arcs follow roughly the general behaviour of SKR. A typical arc extends from 100 to 700kHz, has a vertex around 400kHz with symmetrical curvature around this vertex (Fig.2 in Thieman and Goldstein, 1981). The total duration ranges from 10 to 40 minutes, with an average of about 30 minutes. There is no apparent difference between the form of VE and VL arcs. SKR is not organized entirely into arc patterns as apparently is the case for Jupiter's emissions (Warwick, et al., 1979). Generally only a few arcs are observed within a rotation. Most often these arcs appear isolated, but sometimes nested arcs can also be observed, separated by 15 to 40 minutes.

Before the two encounters when observations were made from above the Saturnian dayside, VE arcs were predominant. After the encounters, observations from above the night hemisphere show that VL arcs prevail (Boischot et al., 1981). Figure 12 illustrates this for Voyager-1. This figure also shows that the predominant species is preferentially observed

in the SLS range where the overall emission probability is the lowest (e.g. compare with Figure 4), whereas the less frequent type appears principally in the SLS range where this probability is the highest. This latter type is generally observed at higher frequencies than the former. In contrast to Jupiter, no evident repetition of the arc pattern is observed from one rotation to the next one.

Low frequency radio emissions --- In the low frequency regime of a few kilohertz, Saturn emits low level electromagnetic nonthermal "continuum" radiation (to use the terminology first applied to the terrestrial spectrum) in addition to SKR. At frequencies below about 2 or 3 kHz, these emissions are trapped within the magnetospheric cavity since the wave frequency is less than the surrounding solar wind electron plasma frequency, f_p. Since electromagnetic waves cannot propagate below f_p, they are refracted away from the relatively high density walls of the magnetopause and are, therefore, trapped within the cavity. Waves generated at a frequency greater than typically 2 to 3 kHz will escape directly into the solar wind.

Figure 13 shows an example of Saturn's trapped radiation. The lower panel is a frequency-time spectogram. The intense band near 300 Hz and the narrowband tones at 2.4 kHz and 700 Hz are spacecraft interference. The broad feature between 500 Hz and 4 kHz is the trapped radiation. The low frequency cutoff of the continuum radiation corresponds very closely to the local f_p (inside the magnetosphere) as derived from the Voyager plasma instrument (Bridge et al.,1981). The electron gyrofrequency, f_g, is about 170 Hz based on measurements by the Voyager magnetic field instrument (Ness et al.,1981). Hence, the emission lies well above $f_g$and has a cutoff very close to f_p thus is most likely an electromagnetic mode. As indicated by the dashed line in the upper panel the radiation has a spectral index of about -3, however, this has been observed to vary between -2.5 and -4.0. This trapped component is not as pervasive or intense at Saturn as it is at Jupiter (Kurth et al., 1982a); however, the spectral density is similar to that at the earth.

The escaping component of Saturn's low frequency radiation was first

described by Gurnett et al. (1981a) who used the term narrowband electromagnetic radi tion because of the narrowbanded nature of the emission. Figure 14 shows spectograms taken from both Voyager-1 and Voyager-2 at a distance of 3 R_s. Although the Voyager-1 spectrum is certainly more complex than that of Voyager-2, both show evidence of narrowband emissions with bandwidths in some cases as small as 1% of the center frequency. For the Voyager-1 spectrum, f_p and f_g were 2.4 kHz and 25.3 kHz, respectively, hence the bands above 2.4 kHz must be propagating in the free space electromagnetic ordinary (L-O) mode. The Voyager-2 spectrum was obtained in a region where f_g was 31 kHz (Ness et al., 1982) and f_p was 2.2 kHz (Bridge et al., 1982) so the very intense band at 6 kHz is apparently propagating in the same mode.

There is evidence that the narrowband emissions extend to as high as 80 kHz. Warwick et al. (1981) report narrowband emissions which were observed to be RH polarized throughout the Voyager-1 near-encounter period. Warwick et al. (1982) report observations by Voyager-2 of a similar narrowband component near 40 kHz, although the observed polarization was LH during that encounter.

2.2 SATURN ELECTROSTATIC DISCHARGES

For a few days around both Voyager encounters with Saturn, the PRA instrument recorded intense, short duration bursts of radio emission quite unlike the magnetospheric emissions described above. Figure 15a shows a dynamic spectrum recorded just at Voyager-1 closest approach. The SKR can be seen as the dark patch of emission cente.ed at about 500 kHz. The unusual emissions are the short, vertical streaks which are present throughout both the PRA low frequency and high frequency bands. Warwick et al. (1981) ruled out any sort of spacecraft interference or nearby discharging as the source of these bursts concluded that the emissions were propagating to the spacecraft from the vicinity of Saturn. They coined the term "SED" for Saturn Electrostatic Discharges.

Burst description -- As can be seen in Figure 15a, each individual SED

appears on only a few consecutive PRA channels, yet SED are observed throughout the entire frequency range. Warwick et al. (1981) concluded that the SED were short duration (tens of milliseconds) bursts with a very large bandwidth (> 40 MHz). Since the PRA receiver steps from one frequency to the next every 30 msec, SED are detected only on the few channels being sampled during the 30 to 250 msec duration of a typical burst. Thus, the length of a streak in Figure 15a reflects the duration of an SED burst (the entire vertical axis of the figure is swept through in 6 seconds). One series of very high time resolution measurements at 10 MHz (a PRA alternate operating mode) showed that individual SED events like those of Figure 15a are made up of many very short (< 1 msec) bursts superimposed on a strong "continuum" (Warwick et al.,1981). Some structure at the time resolution limit of 140 microseconds (in the high rate mode) led Warwick et al. (1981) to estimate that the SED source was no larger than 40 km in size.

Figure 16 shows the distribution of SED durations during both the Voyager-1 and Voyager-2 encounter periods. Both sets of data are extremely well fit by an equation of the form

$$N = N_o \exp(-D/D_o)$$

where N is the number of SED bursts, and D is their duration in milliseconds. Least squares fits give values of D_o of 40 ± 1 and 37 ± 2 msec for the overall Voyager-1 and Voyager-2 encounters, respectively. The value of D_o at closest approach was about 58 msec, because proximity to the source allows weak emission at the beginning and end of an SED burst to be detected, and this has the effect of lengthening the average SED burst. The maximum rate of SED detected by Voyager-1 at closest approach was about 0.2 per second, and the distribution of the number of SED per unit time was well matched by a Poisson distribution (Evans, et al., 1983). Figure 16 also shows that the absolute occurrence of SED appears to be reduced by about a factor of 3 for the Voyager-2 encounter as compared to Voyager-1, in agreement with the findings reported by Warwick et al. (1982). However, the PRA receiver on Voyager-2 was operating with 15 dB of attenuation during the ten hours centered on closest approach which probably accounts

for much of the difference between the total number of SED detected by the two spacecraft.

The total power dissipated in an SED burst has been estimated to be 10^7 to 10^8 W by Warwick et al. (1981), and as high as 10^{10} W during some events (Evans et al., 1983; Zarka and Pedersen, 1983). Total power is somewhat difficult to estimate because of the lack of knowledge of the instantaneous bandwidth and spectral shape of SED bursts. For the estimates appearing in the literature, the authors have used a bandwidth of 40 to 100 MHz and have assumed that the spectrum is flat. If SED are indeed as powerful as 10^{10} W, then ground based radio telescopes suitably equipped should be able to monitor SED.

Knowledge about the polarization of SED is confused at best. Evans et al. (1981) reported that most SED bursts observed by Voyager-1 during the inbound trajectory were unpolarized, but, during the outbound leg, LH polarization was observed particularly at frequencies above 15 MHz. Zarka and Pedersen (1983) cautioned that the PRA antenna system does not measure polarization very reliably above 15 MHz, and suggested the possibility that SED may be unpolarized at all times.

Kaiser et al. (1983) analyzed the SED observations and found that SED were actually observed in the PRA low band only after the spacecraft had passed Saturn and were making observations from above the night hemisphere. Observations of SED during the inbound legs above the daylit hemisphere (see Figure 1) never showed bursts below about 5 MHz (see Figure 20a).

Episode periodicity -- One of the most revealing aspects of the SED observations was the grouping of individual SED into episodes which recurred with a distinct periodicity of about 10h 10m (Voyager-1), quite different from the 10h 39.4m Saturn rotation period deduced from SKR observations. These episodes appeared for a few days on either side of closest approach. The phase of the SED repetition period was found to be fixed relative to the line between planet and observer, implying that the source of SED rotates or revolves like a searchlight, and is not fixed

relative to the sun, as is the case for SKR (Warwick et al., 1982). Zarka and Pedersen (1983) showed that the repetition of episodes for the Voyager-2 encounter were marginally faster (10h 00m) than for the Voyager-1 encounter, but both periodicities have relatively large uncertainties.

Kaiser et al. (1983) showed that the number of SED fell to zero for three-hour periods in between episodes. This on-off behavior was quite different from the SKR which waxes and wanes with its 10h 39.4m period but does not generally disappear. This pattern is depicted schematically for Voyager-1 in Figure 20a. The occurrence rate of SED during a given "on" period, however, is not uniform. An episode may contain several relative maxima and minima (e.g. see "double hump" episode described by Evans et al.,1981), although the general trend is for a build up of the number of SED per unit time followed by a subsequent decline before total disappearance.

An additional puzzling aspect of the SED episodes was first reported by Evans et al. (1981), and concerned the onset of the episodes as a function of frequency. During all episodes but one, the onset of each episode was approximately independent of frequency. The lone exception was the episode which began just before the Voyager-1 closest approach where SED were first observed in the 30 to 40 MHz band and slowly, over a four hour interval, filled the PRA receiver down to the lowest frequency (Figure 20a). Kaiser et al. (1983) counted the number of SED in the 30 to 40 MHz band as a function of time during this frequency dependent onset and reported that the rate increased from one SED every 20-30 seconds to the maximum rate of one per 5 seconds over the same 4 hour interval required for the SED to spread throughout the entire PRA bandwidth.

3.0 DISCUSSION

3.1 INFERRED SOURCE LOCATIONS

3.1.1 SKR

The observation of predominantly RH polarized emission during the northern hemisphere inbound Voyager-1 trajectory led Kaiser et al. (1980) to conclude that the radio source was in the northern hemisphere and that the radiation was escaping in the right-hand extraordinary (R-X) mode. This conclusion was founded on the assumption that the emission was being observed directly and not by way of a back lobe of the radiation pattern. It was also necessary to know, of course, that Saturn's main magnetic field, like Jupiter's, has its field lines emanating from the planet's northern hemisphere (Acuna et al., 1980; Smith et al., 1980).

Post encounter Voyager observations of the same RH polarized radio source showed that the subspacecraft SLS longitude of maximum detection probability had shifted by an amount equal to the local time change of the spacecraft. This important piece of data indicated that the source was locked in local time, that is, emitting radiation into the same directions relative to the sun whenever a particular magnetic longitude reached a fixed solar hour angle (Warwick et al., 1981; Gurnett et al., 1981). A 'searchlight' type of radio source, one that rotates with the planet emitting all the time, was thus excluded by the observations. Only when the detection probability is a maximum at the same magnetic longitude regardless of observer local time is such a source indicated. Subsequent observation of a distinct LH polarized source at a time when Voyager-1 was south of Saturn's equator plane was taken as evidence of a southern-hemisphere source, also emitting in the R-X magnetoionic mode (Warwick et al., 1981) and similarly locked into the dayside local time hemisphere.

These general conclusions regarding the hemisphere locations of the radio sources were later confirmed by Kaiser, Desch and Lecacheux (1981) and by Kaiser and Desch (1982) and Lecacheux and Genova (1983) who quantitatively modeled the precise source locations. In the first two of these papers, the observed ratios of pre encounter to post encounter radiation intensities were compared with the ratios that would be expected from beams located at many different places. The beam locations were not constrained in any way in the space around Saturn, but the beam axis

orientation was required to be aligned with the magnetic field direction. The source altitude was set by assuming that emission took place at or near the local f_g. As had previously been concluded, the RH polarized source was found to be in the northern hemisphere and the LH polarized source in the southern. Further, Kaiser and Desch showed that for the northern hemisphere source, only radio sources on those magnetic field lines whose footprints were constrained to about 70^o to 80^o latitude, 100^o to 130^o SLS longitude and 10 to 12 hr local time could satisfy the SKR observations. The southern hemishere was less tightly constrained to about -60^o to -85^o latitude, 300^o to 75^o SLS longitude, and 7 to 16 hr local time. The footprint of the Kaiser and Desch source regions are shown in Figure 17. Lecacheux and Genova (1983) found essentially the same source locations by studying the changes in the visibility of the two sources (RH and LH) as viewed from the spacecraft trajectories. It is important to note that these source locations are consistent with the surface locations of Saturn's UV aurorae (Sandel et al., 1982), polar cap boundary (Ness et al., 1981), and polar cusp (Behannon et al., 1981). Thus the source locations correspond to active regions in Saturn's magnetosphere, where the field lines tend to open up into the interplanetary medium and where intense particle precipitation and auroral stimulation occur. Localization of the source footprints in these high latitude dayside regions of the magnetosphere is thus consistent with the strong SKR-solar wind correlation observed by Desch (1982).

Taken as a whole, there now seem to several independent lines of evidence to suggest the existence of some irregularity or inhomogeneity in Saturn's high latitude regions; in the northern hemisphere this inhomogeneity is probably near 115^o SLS. The very existence of some source of rotation (10.66 hr) modulation of SKR, the localization of the radio sources to specific longitude ranges on the planet, and a similar confinement of the auroral activity all suggest a magnetic influence, possibly in the form of a magnetic anomaly in the near-surface field. However no direct evidence of such an anomaly exists (see Connerney et al. this book). Saturn's global field is modelled to be azimuthally symmetric and lacks any substantial tilt away from the spin axis. This inability to account for magnetic longitude confinement of the aurorae and of the radio

sources remains one of the major problems confronting Saturn investigators.

3.1.2 Low-frequency emissions

The source location of the escaping narrowband emissions is not well known due to the small number of observations and also because there is no appreciable tilt in the magnetic dipole axis which might have permitted one to look for geometry-dependent propagation effects. Figure 18 shows the position of the Voyager spacecraft at times when narrowband emissions could be observed in the frequency range of 5 to 15 kHz. The two filled boxes represent the position of the spacecraft when the emissions were strongest and correspond to times represented by the two spectra shown in Figure 14. The open boxes represent the detection of relatively weak narrowband emissions, primarily near 5 - 6 kHz. Gurnett et al. (1981b) reported a periodicity in the detection of this 5 - 6 kHz band which is close to that of Saturn's rotation period. The maximum intensity occurs when the spacecraft SLS longitude is near 290°. The observations depicted in Figure 18 are consistent with a source near Saturn which illuminates high latitudes. Low latitudes are shielded by the high-density plasma sheet.

Gurnett et al. (1981b) also suggested another possibile method for determining the source location of the escaping narrowband emissions. They noticed several different frequency spacings between the bands seen in the Voyager-1 spectrum shown in Figure 14 and made the assumption that the spacing is related to f_g at the source. Three such sets of harmonically spaced lines were identified with the values of f_g at radial distances of 5.4, 7.3, and 8.8 Saturn radii. These are near the orbits of Tethys, Dione, and Rhea. Gurnett et al. (1981b) conjectured the source of the escaping narrowband radiation was associated with the L-shells of these moons and probably located above or below the equatorial plane on a density gradient of the plasma sheet. The bottom panel of Figure 19 is a schematic representation showing one possible geometry implied by Gurnett et al. (1981b). Here, the Dione L-shell is shown as a preferred region and electrostatic waves near the upper hybrid resonance, $f_{UHR} = (f_p^2 + f_g^2)^{1/2}$ lying on the density gradient of the plasma sheet are thought to be the source of the electromagnetic emissions. This geometry also favors emission

towards high latitudes.

The trapped component of the low frequency spectrum was detected at relatively high latitudes (>20°) both above and below the equator in low density regions of the pre-dawn magnetosphere (Kurth et al., 1982a). This geometry is consistent with the magnetotail lobes where a similar type of radiation is most prevalent at the earth and Jupiter. By analogy with the earth and Jupiter, the radiation is probably emitted in a manner similar to the narrowband emissions near f_{UHR} located on density gradients.

3.1.3 SED

Only two known locations in the Saturn system have rotation or revolution periods comparable to the 10h 10m SED episode periodicity. One possible location, first suggested by Burns et al. (1983), is in the cloud tops of the equatorial atmosphere, where the Voyager imaging results (see chapter by Ingersoll et al.) showed wind velocities of 500 m/s, corresponding to a rotation period of the atmosphere at that latitude of about 10h 10m. The other location is at 1.8 R_s, in the middle of Saturn's B ring, where the Keplerian revolution period is 10h 10m. Warwick et al. (1981) and Evans et al. (1981, 1982, 1983) concluded that the SED were generated by an object in the B ring undergoing successive discharging. They reasoned that since SED were sometimes observed to frequencies well below 1 MHz (see Figure 15a), the atmospheric location could be ruled out because the Saturnian ionosphere would prevent escape of frequencies that low (see chapter by Atreya et al.).

Burns et al. (1983) compared the characteristics of SED with the properties of lightning at the earth, Jupiter, nd Venus and suggested that SED bursts criginated from atmospheric lightning in the Saturnian equatorial region They proposed that the emission escaped through a long-lived ionospheric hole created by the shadow of the ring system. Kaiser et al. (1983) noted that since SED bursts below 5 MHz were not observed when Voyager was above the dayside, and low frequency SED appeared only over the nightside, the justification used by Warwick et al. (1981) for ruling out the atmosphere was not as clear as previously assumed. They suggested that if the

ionospheric plasma density near the noon meridian was ~3 X 10^5 cm^{-3}, escape of atmospheric radio bursts below 5 MHz would be prevented. They further stated that if the nighttime ionosphere had low density regions or "holes", the observed low frequency emissions could escape.

However, the day-night frequency extent argument for placing the source of SED in the equatorial atmosphere was secondary to the major argument presented by Kaiser et al. (1983). They pointed out that the on-off pattern of SED episodes was the signature to be expected from a source undergoing consecutive occultations by the planet. During the three-hour intervals when SED bursts were absent, they reasoned that the source of SED was out of view of Voyager, behind the planet. The on-off pattern is shown schematically in Figure 20a. They were then able to calculate what the expected occultation pattern for a point source in the B ring would be, and this is shown in Figure 20d. Clearly, the predicted SED "off" periods for a ring source are much shorter than those observed. Conversely, a single point source in the equatorial atmosphere should have much longer off times than observed (Figure 20c). Figure 20b shows the occultation pattern predicted by an extended storm system aligned so that the onset of the first episode in the figure corresponds to the storm system coming into view over the limb. This panel shows that the only solution to the occultation pattern was for a storm in the equatorial atmosphere extended some 60° in longitude. Kaiser et al. (1983) were also able to show that the storm was confined to within a few degrees of the equator, because of the small spread ($\pm$5 min) in the repetiton period.

The atmospheric storm source location of Kaiser et al. (1983) also explains the odd frequency-dependent episode onset at Voyager-1 closest approach. Figure 21 shows the trajectory of Voyager-1 past Saturn with three insets depicting the view of Saturn from the spacecraft at the indicated times. In inset (a), the equatorial storm system is just coming into view around the planet's morning terminator. At this time, however, the Voyager-1 spacecraft is moving so fast around Saturn that it nearly co-rotates with the planet. Thus, the storm takes a much longer time to rise, namely about four hours, than during any other episode. The radio emission from the lightning bursts necessarily travel through the dayside ionosphere before

reaching the spacecraft, and experience frequency-dependent refraction in the process. The low frequencies are either blocked completely, or are strongly refracted away from Voyager-1. The highest frequencies above 20 MHz, however, suffer very little refraction and can propagate to the spacecraft in more or less a straight line. Voyager-1 then observes first the high frequencies and slowly over the four-hour interval successively lower and lower frequencies, until by the time of inset (b), the entire PRA frequency range can be viewed. Inset (b) also corresponds to the first occasion that Voyager-1 had to observe the storm on the nightside of Saturn. By the end of the episode shown in inset (c), Voyager-1 is no longer co-rotating with Saturn, so the source quickly sets over the dawn meridian.

3.2 EMISSION THEORIES

3.2.1 SKR

There are two phenomena that relate to SKR which have received attention from theorists. The first is the occurrence of the radio emission itself. The theoretical work in this area has not been done specifically for Saturn, but rather for the earth's AKR. The second area of interest for the theorists is the formation of discrete arcs in the dynamic spectra of both Saturn and Jupiter.

Grabbe (1981) presents a review of the theories for generation of AKR. All of these theories make use of the observed correlation between AKR and auroral electron precipitation. Intense beams of electrons in the few keV energy range are presumed to be the energy source for SKR. The theories are then concerned with just how this energy source gets converted into electromagnetic radiation. The AKR theories are divided into two categories, direct processes and conversion processes. The direct process theories convert the energy in the electron beam directly into an escaping electromagnetic mode without going through intermediate steps. The

conversion process theories first convert the electron beam energy into an electrostatic mode which then subsequently gets converted into an escaping electromagnetic mode. Of the 15 or so theories proposed for AKR generation, many have been ruled out by more recent measurements, particularly those which have determined that AKR is emitted primarily in the R-X mode and not the L-O mode (see Shawhan and Gurnett 1982)). Only those AKR theories which are still viable as of this writing and which might have application at Saturn will be described. Since SKR is observed to be RH polarized above Saturn's Northern hemisphere and LH above the Southern hemisphere, Warwick et al. (1981) have concluded that, like AKR, SKR is emitted in the R-X mode.

A problem for the direct process theories has been how to get the emission up to high enough frequency to escape. AKR is observed to be generated in regions where $f_p < 0.2\, f_g$ (Calvert, 1981), but the emission can only escape at frequencies above the R-X cutoff which is just above f_g. The direct process theories make use of an idea originally proposed by Ellis (1962), Ellis and McCulloch (1963), and Melrose (1973,1976). This idea uses the beam velocity to Doppler shift the emission, which is presumed to be generated at the local f_g value, to above the R-X cutoff.

Two recent theories show considerable promise in explaining much of the AKR phenomenology and could possibly be applied to Saturn's magnetospheric cusp or dayside auroral region. Wu and Lee (1979) and Lee, Kan and Wu (1980) make use of a loss cone distribution (i.e. a distribution with low parallel velocity particles absent) which has been reported for the earth's auroral electron beams. They determine that the free energy of this loss cone distribution can preferentially drive R-X mode radiation, and can produce the observed power levels. Grabbe et al. (1980), on the other hand, propose that the electromagnetic noise interacts with low frequency coherent density fluctuations (which are created by electrostatic ion cyclotron waves). The result is a three wave process in which beat waves are produced which interact with the electron beam. When the wave frequency is just below the Doppler shifted beam f_g, the R-X mode emission undergoes a convective instability and wave growth occurs.

The major problem with the conversion process theories is that very high efficiency is required in each of the conversion steps so that the observed AKR power levels can be obtained from the energy available in the electron beam. One theory may be applicable to SKR. Roux and Pellat (1979) and James (1980) proposed a coherent three wave process in which two electrostatic waves combine to produce the observed electromagnetic wave. The best candidate waves for the resulting R-X mode emission are whistler waves at frequencies above the lower hybrid resonance, and so-called Z mode waves in the range from f_g to f_{UHR}.

Application of any of these theories to Saturn is strictly an arm-chair science, since no observations have been made in situ in Saturn's auroral zones or magnetospheric cusps. However, by analogy with the earth, we can conjecture that conditions may well be similar.

The dynamic spectral arcs described in section 2.2.1 show many similarities to arcs in the decameter wavelength range observed at Jupiter (Warwick, et al., 1979). Two of the theories put forth to explain the Jovian arcs may be applicable to Saturn. The first theory (Pearce, 1981; Goldstein and Thieman, 1981) proposes that emission (Jovian) is beamed into a thin conical sheet. Rotation causes this beam to sweep past the observer so that emission is detected at a given frequency only when the line of sight is parallel to the sides of the conical sheet. Emission cones at successive frequencies have slightly differing orientations because they emanate from different points on a field line where the emission frequency is close to the local f_g. The combination of all these beams can produce the arc patterns observed. A major problem with this theory is the observation that the SKR source does not rotate with the planet, but stays fixed with respect to the sun. Thieman and Goldstein (1981), however, believe that the SKR beam need only rotate through a relatively small angle for the mechanism to work.

The other theory (Lecacheux et al., 1981) suggests that arcs are caused by diffraction of radio waves as they pass through a phase changing plasma structure. In the case of Jupiter, this plasma structure is the Io plasma torus which nods up and down (relative to the observer) with the rotation

of the planet's tilted magnetic field. For Saturn, no nodding is possible because of the lack of appreciable tilt, but the torus associated with Dione and several other inner satellites (see chapter by Scarf et al.) could contain azimuthal variations in density which may be capable of generating SKR arcs.

3.2.2 Low frequency emissions

For the case of the earth, Kurth et al. (1981a) have demonstrated that both the diffuse, trapped continuum radiation and the narrowband escaping radiation are generated by the same mechanism. Most progress has been made in understanding the source mechanism by studying the higher frequency escaping emissions, since the identity of the escaping emission is preserved by not having undergone multiple reflections within the magnetospheric cavity. A number of theories are currently proposed to explain the generation of continuum radiation. Most of these theories attempt to use intense electrostatic waves near f_{UHR} as the source. The theories generally fall into two categories: linear conversion to L-O mode radiation (Jones, 1976; Okuda et al., 1982; Lembege and Jones, 1982), and nonlinear 3-wave processes using low frequency waves such as the ion-cyclotron mode as the third wave (Melrose, 1981). Barbosa (1982) provides a review of the status of the theories for the terrestrial and Jovian emissions.

Gurnett et al. (1981b) have applied the theoretical work done for the earth and Jupiter to the Saturnian narrowband radiation. The schematic at the top of Figure 19 shows the essential ideas of the emission mechanism. Kurth et al. (1979) established that intense electrostatic bands could often be detected at or near the terrestrial plasmapause when $f_{UHR} = (n+1/2)\, f_g$. These are the upper hybrid waves commonly thought to be the source of the continuum radiation. Since evidence for the conversion from these electrostatic bursts to electromagnetic radiation is found primarily at a density gradient such as the plasmapause, and the conversion theories rely on a density gradient to enable the electromagnetic waves to escape, Gurnett et al. (1981b) proposed that the low-frequency Saturnian emission is generated on the gradient at the edge of the plasma sheet. In this case,

the gradient is approximately parallel to the magnetic field direction as can be seen in the bottom panel of Figure 19. This is opposite to the geometry that exists at the earth's plasmapause or the Io torus at Jupiter. This new geometry has not been analyzed theoretically to determine if the emission generation would proceed as in the more familiar perpendicular case. Alternatively, one could identify density gradients associated with the plasma sheet which are aligned nearly perpendicular to the magnetic field and which might be more suitable sites for the narrowband generation (see Fig. 6b of Gurnett et al. [1981b]).

The ordinary mode inference by Gurnett et al. (1981b) is consistent with the linear conversion theory which predicts predominantly L-O mode radiation. It is difficult to establich the consistency of the polarization observations of Warwick et al. (1981) (RH) and Warwick et al. (1982) (LH) since knowledge of the source location and field direction is required to relate these observations to a magnetoionic mode. Some mixture of modes, particularly in the trapped radiation, may be expected since both ordinary and extraordinary modes are commonly detected at the earth. There it is thought the radiation is primarily in the L-O mode and subsequent mode converison is responsible for the R-X component.

3.2.3 SED

Virtually all researchers working with the SED data agree that the emission is produced by a discharge phenomenon. Warwick et al. (1981, 1982) and Evans et al. (1981,1982,1983) proposed discharges by an unknown object within the Saturnian rings, although Kaiser et al. (1983) have shown that much of the work concerning the ring source (e.g. frequency extent and on-off episode structure) was based on incomplete analysis of the original data. Burns et al. (1983) and Kaiser et al. (1983) proposed that SED are the radio counterpart of atmospheric lightning flashes. Table 2, adapted from Burns et al. (1983), compares some of the properties of SED with lightning "observations" at Jupiter, Venus and the earth. Many of the values in the table are poorly known. The quantities at both Jupiter and Venus have, in many cases, been deduced by using indirect observations and some assumptions. In the case of the earth, there is an overwhelming amount

of data, but most of this data is concerned with cloud to ground lightning strokes, whereas, for comparison with SED, we are more interested in cloud to cloud strokes. Nevertheless, Table 2 suggests that SED bursts have many of the same properties as atmospheric lightning bursts. A good tutorial on discharge phenomena as applied to terrestrial lightning may be found in the text by Uman (1969).

The flash rates listed in Table 2 correspond to about 100 flashes per second for the earth and 8 to 80000 flashes per second for Jupiter, thus the possibility of SED-like bursts from those planets should be investigated. Preliminary examination of the Voyager data obtained during the periods immediately following the launches in 1977 and the Jupiter encounters in 1979 has failed to reveal any signatures resembling SED. The reasons for this lack of detection are beyond the scope of this review, but should be studied as soon as possible.

3.3 THE FUTURE

We have seen an explosion in knowledge of Saturn's magnetosphere since 1979, and much remains to be done with the Pioneer 11 and Voyager data sets. However, it seems as of this writing that there will be no new data recorded *in situ* from Saturn's magnetosphere during the remainder of this century. Thus, further progress in some areas of Saturn-related research will necessarily suffer. In the radio astronomy of Saturn, it is hoped that some additional insights can be gained by studying the radio emissions of the earth and Jupiter. We have alluded to the similarities of some of the radio components from these three planets throughout this chapter, and there are likely other similarities to be found. Thus, one or more of the theories put forth to explain AKR may successfully be adapted to both Jupiter and Saturn. If that happens, we will perhaps then be in a position to "invert" the radio data and deduce just what conditions exist at the emission generation sites deep within the magnetospheres of these planets.

Acknowledgments

The authors thank J.K. Alexander for many valuable and constructive comments. The research at the University of Iowa was supported by the National Aeronautics and Space Administration through contract 954013 with the Jet Propulsion Laboratory. The research at the Paris Observatory in Meudon was supported by the Centre National d'Etudes Spatiales. The research at Radiophysics, Inc. is supported by the National Aeronautics and Space Administration through contract NAS 7-100 with the Jet Propulsion Laboratory.

Table 1: Comparison of Saturn Radio Components

PROPERTY	SKR	SED	Low Frequency Emissions (escaping)	(trapped)
Frequency Range	3 kHz-1200 kHz	~20 kHz- >40 MHz	3-100 kHz	300Hz-3kHz
Total Power (isotropic)	10^8-10^{10} W	10^7-10^{10} W	~10^6 W	~10^7 W
Polarization	RH (northern) LH (southern)	Usually un-polarized, sometimes mixed	ordinary mode	?
Dynamic Spectral Character	spectral arcs + other complex features	broadband	narrowband	amorphous
Recurrence Periods	10h 39.4m 25d	~10h 10m	~10h 40m	none
Origin	low to mid altitude dayside polar cusps	Atmospheric Lightning	near plasma sheet gradients	

Table 2. Properties of planetary lightning and SED

PROPERTY	VENUS	EARTH	JUPITER	SATURN (SED)
Flash rate (km^{-2} yr^{-1})	>0.08 (R) 0 - 45 (O)	2 - 7 (O)	4 - 40 (R) 4 X 10^{-3} (O)	0.02 (10^{-4})*
Event Duration	250 msec	34 msec	< 35 sec	30 - 450 msec
Stroke Duration	?	~ 1 msec	?	~ 1 msec
Energy per flash (J)	7 X 10^{7} (O)	4 x 10^{8} (total)	2.5 X 10^{9} (O)	10^{7} - 10 (R)

O = Optical
R = Radio

* -- Values for the assumed 60^{o} X 4^{o} storm area and (in parentheses) for the entire planet.

References

Acuna, M.H.; and Ness, N.F. 1980. The magnetic field of Saturn: Pioneer 11 observations. Science 207: 444-446.

Acuna, M. H.; Ness, N. F.; and Connerney, J. E. P. 1980. The magnetic field of Saturn: Further studies of the Pioneer 11 studies. J. Geophys. Res. 85: 5675-5678.

Alexander, J.K; Carr, T.D.; Thieman, J.R.; Schauble, J.J.; and Riddle, A.C. 1981. Synoptic observations of Jupiter's radio emissions: average statistical properties observed by Voyager. J. Geophys. Res. 86: 8529-8545.

Barbosa, D.D. 1982. Low level VLF and LF radio emissions observed at earth and Jupiter. Rev. Geophys. Space Sci. 2: 316-334.

Behannon, K.W.; Connerney, J.E.P.; and Ness, N.F. 1981. Saturn's magnetic tail: structure and dynamics. Nature 292: 753-755.

Boischot, A.; Leblanc, Y.; Lecacheux, A.; Pedersen, B.M.; and Kaiser, M.L. 1981. Arc structure in Saturn's radio dynamic spectra. Nature 292: 727-728.

Bridge, H.S.; Bagenal, F.; Belcher, J.W.; Lazarus, A.J.; McNutt, R.L.; Sullivan, J.D.; Gazis, P.R.; Hartle, R.E.; Ogilvie, K.W.; Scudder, J.D.; Sittler, E.C.; Eviatar, A.; Siscoe, G.L.; Goertz, C.K.; and Vasyliunas, V.M. 1982. Plasma observations near Saturn: initial results from Voyager 2. Science 215: 563-571.

Bridge, H.S.; Belcher, J.W.; Lazarus, A.J.; Olbert, S.; Sullivan, J.D.; Bagenal, F.; Gazis, P.R.; Hartle, R.E.; Ogilvie, K.W.; Scudder, J.D.; Sittler, E.C.; Eviatar, A.; Siscoe, G.L.; Goertz, C.K.; and Vasyliunas, V.M. 1981. Plasma observations near Saturn: initial results from Voyager 1, Science 212: 217-225.

Brown, L.W. 1975. Saturn radio emission near 1 MHz. Astrophys. J. 198: L89-L92.

Burns, J.A.; Showalter, M.R.; Cuzzi, J.N.; and Durisen, R.H. 1983. Saturn's electrostatic discharges: could lightning be the cause? Icarus 54: 280-295.

Calvert, W. 1981. The auroral plasma cavity. Geophys. Res. Lett. 8: 919-91.

Carr, T.D.; Schauble, J.J.; and Schauble, C.C. 1981. Pre-encounter distributions of Saturn's low frequency radio emission. Nature 292: 745-747.

Carr, T.D.; Smith, A.G.; Bollhagen, H.; Six, N.F.; and Chatterton, N.E. 1961. Recent decameter wavelength observations of Jupiter, Saturn, and Venus. Astrophys. J. 134: 105-125.

Desch, M. D. 1982. Evidence for solar wind control of Saturn radio emission. J. Geophys. Res. 87: 4549-4554.

Desch, M.D.; and Kaiser, M.L. 1981a. Voyager measurement of the rotation period of Saturn's magnetic field. Geophys. Res. Lett. 8: 253-256.

Desch, M. D.; and Kaiser, M. L. 1981b. Saturn's kilometric radiation: satellite modulation. Nature 292: 739-741.

Desch, M. D.; and Rucker, H. C. 1983. The relationship between Saturn Kilometric Radiation and the solar wind. J. Geophys. Res., in press.

Ellis, G.R.A. 1962. Cyclotron radiation from Jupiter. Aust. J. Phys. 15: 344-353.

Ellis, G.R.A.; and McCulloch, P.M. 1963. The decametric radio emissions of Jupiter. Aust. J. Phys. 16: 380-397.

Evans, D.R.; Romig, J.H.; Hord, C.W.; Simmons, K.E.; Warwick, J.W.; and Lane, A.L. 1983. The source of Saturn electrostatic discharges. Nature 299: 236-237.

Evans, D.R.; Romig, J.H.; and Warwick, J.W. 1983. Saturn electrostatic discharges: properties and theoretical considerations. Icarus 54: 267-279.

Evans, D.R.; Warwick, J.W.; Pearce, J.B.; Carr, T.D.; and Schauble, J.J. 1981. Impulsive radio discharges near Saturn. Nature 29: 716-718.

Gallagher, D.L.; and Gurnett, D.A. 1979. Auroral kilometric radiation: time-averaged source location. J. Geophys. Res. 84: 6501-6509.

Genova, F.; Pedersen, B.M.; and Lecacheux, A. 1983. Dynamic spectra of Saturn kilometric radiation. J. Geophys. Res.: in press.

Goldstein, M.L.; and Thieman, J.R. 1981. The formation of arcs in the dynamic spectra of Jovian decameter bursts. J. Geophys. Res. 86: 8569-8578.

Grabbe, C.L. 1981. Auroral kilometric radiation: a theoretical review. Rev. Geophys. Space Sci. 19: 627-634.

Grabbe, C.L.; Palmadesso, P.; and Papadopoulos, K. 1980. A choerent nonlinear theory of auroral kilometric radiation: 1. steady state model. J. Geophys. Res. 85: 3337-3346.

Gurnett, D.A. 1974. The earth as a radio source: terrestrial kilometric radiation. J. Geophys. Res. 79: 4227-4238.

Gurnett, D.A.; Kurth, W.S.; and Scarf, F.L. 1981a. Plasma waves near Saturn: initial results from Voyager 1. Science 212: 235-239.

Gurnett, D.A.; Kurth, W.S.; and Scarf, F.L. 1981b. Narrowband electromagnetic emissions from Saturn's magnetosphere. Nature 292: 733-737.

Haerendel, G.; Paschmann, G.; Sckopke, N.; Rosenbauer, H.; and Hedgecock, P. C. 1978. The frontside boundary layer of the magnetosphere and the problem of reconnection. J. Geophys. Res. 83: 3195-3216.

James, H.G.; 1980. Measurements of auroral kilometric radiation and associated ELF data from Isis I. J. Geophys. Res. 85: 3367-3375.

Jones, D. 1976. Source of terrestrial nonthermal radiation. Nature 260:

686-688.

Kaiser, M.L. 1976. A low-frequency radio survey of the planets with RAE 2. J. Geophys. Res. 82: 1256-1260.

Kaiser, M. L.; and Desch, M. D. 1982. Saturnian kilometric radiation: source locations. J. Geophys. Res. 87: 4555-4559.

Kaiser, M.L.; Connerney, J.E.P.; and Desch, M.D. 1983. Atmospheric storm explanation of saturnian electrostatic discharges. Nature 303: 50-53..

Kaiser, M.L.; Desch, M.D.; and Lecacheux, A. 1981. Saturnian kilometric radiation: statistical properties and beam geometry. Nature 292: 731-733.

Kaiser, M.L.; Desch, M.D.; Warwick, J.W.; and Pearce, J.W. 1980. Voyager detection of nonthermal radio emission from Saturn. Science 209: 1238-1240.

Kurth, W.S.; Craven, J.D.; Frank, L.A.; and Gurnett, D.A. 1979. Intense electrostatic waves near the upper hybrid resonance frequency. J. Geophys. Res. 84: 4145-4154.

Kurth, W.S.; Gurnett, D.A.; and Anderson, R.R. 1981b. Escaping nonthermal continuum radiation. J. Geophys. Res. 86: 5519-5531.

Kurth, W. S.; Gurnett, D. A.; and Scarf, F. L. 1981a. Control of Saturn's radio emission by Dione. Nature 292: 742-745.

Kurth, W.S.; Scarf, F.L.; Sullivan, J.D.; and Gurnett, D.A. 1982a. Detection of nonthermal continuum radiation in Saturn's magnetosphere. Geophys. Res. Lett. 9: 889-892.

Kurth, W.S.; Sullivan, J.D.; Gurnett, D.A.; Scarf, F.L.; Bridge, H.S.; and Sittler, E.C. 1982b. Observations of Jupiter's distant magnetotail and wake. J. Geophys. Res. 87: 10373-10384.

Lecacheux, A.; and Genova, F. 1983. Localization of Saturn's radio sources. J. Geophys. Res., in press.

Lecacheux, A.; Meyer-Vernet, N.; and Daigne, G. 1981. Jupiter's decametric radio emission: a nice problem of optics. Astron. Astrophys. 94: L9-L12.

Lee, L.C.; Kan, J.R.; and Wu, C.S. 1980. Generation of AKR and the structure of auroral acceleration region. Planet. Space Sci. 28: 703-711.

Lembege, B.; and Jones, D. 1982. Propagation of electrostatic upper hybrid emission and Z mode waves at the geomagnetic equatorial plasmapause. J. Geophys. Res. 87: 6187-6201.

Lepping, R.P.; Burlaga, L.F.; and Desch, M.D. 1982. Evidence for a distant (>8700 RJ) jovian magnetotail: Voyager 2 observations. Geophys. Res. Lett. 9: 885-888.

Melrose, D.B. 1973. Coherent gyromagnetic emission as a radiation mechanism. Aust. J. Phys. 26: 229-247.

Melrose, D.B. 1976. An interpretation of Jupiter's decametric radiation and the terrestrial kilometric radiation as direct amplified gyroemission. Astrophys. J. 207: 651-662.

Melrose, D.B. 1981. A theory for the nonthermal radio continua in the terrestrial and Jovian magnetospheres. J. Geophys. Res. 86: 30-36.

Ness, N.F.; Acuna, M.H.; Behannon, K.W.; Connerney, J.E.P.; Lepping, R.P.; and Neubauer, F.M. 1982. Magnetic field studies by Voyager 2: Preliminary results at Saturn. Science 215: 558-563.

Ness, N.F.; Acuna, M.H.; Lepping, R.P.; Connerney, J.E.P.; Behannon, K.W.; Burlaga, L.F.; and Neubauer, F.M. 1981. Magnetic field studies by Voyager 1: preliminary results at Saturn. Science 212: 211-217.

Newburn, R.L. Jr.; and Gulkis, S. 1973. A survey of the outer planets Jupiter, Saturn, Uranus, Neptune, Pluto, and their satellites. Spa. Sci. Rev. 3: 179-271.

Okuda, H.; Ashour-Abdalla, M.; Chance, M.S.; and Kurth, W.S. 1982. Generation of nonthermal continuum radiation in the magnotesphere. J. Geophys. Res. 87: 10457-10462.

Pearce, J.B. 1981. A heuristic model for Jovian decametric arcs. J. Geophys. Res. 86: 8579-8581.

Roux, A.; and Pellat, R. 1979. Conerent generation of the terrestrial kilometric radiation by nonlinear beating of electrostatic waves. J. Geophys. Res. 84: 5189-5198.

Sandel, B. R.; Shemansky, D. E.; Broadfoot, A. L.; Holberg, J. B.; Smith, G. R.; McConnell, J. C.; Strobel, D. F.; Atreya, S. K.; Donahue, T. M.; Moos, H. W.; Hunten, D. M.; Pomphrey, R. B.; and Linick, S. 1982. Extreme ultraviolet observations from Voyager 2 encounter with Saturn. Science 215: 548-553.

Scarf, F.L; and Gurnett, D.A. 1977. A plasma wave investigation for the Voyager mission. Space Sci. Rev. 21: 289-308.

Scarf, F.L.; Gurnett, D.A.; Kurth, W.S.; and Poynter, R.L. 1982. Voyager 2 plasma wave observations at Saturn. Science 215: 587-594.

Shawhan, S.D.; and Gurnett, D.A. 1982. Polarization measurements of auroral kilometric radiation by Dynamics Explorer 1. Geophys. Res. Lett. 9: 913-916.

Smith, A.G.; and Carr, T.D. 1959. Radio frequency observations of the planets in 1957-1959. Astrophys. J. 130: 641-647.

Smith, E.J.; Davis, L.; Jones, D.E.; Coleman, P.J.; Colburn, D.S.; Dyal, P.; and Sonnett, C.P. 1980. Saturn's magnetic field and magnetosphere. Science 207: 407-410.

Smith, H.J. 1959. Nonthermal solar system sources other than Jupiter. Astron. J. 64: 41-43.

Smith, H.J.; and Douglas, J.N. 1957. First results of a planetary radio astronomy program of the Yale Observatory. Astron. J. 62: 247.

Smith, H.J.; and Douglas, J.N. 1959. Observations of planetary nonthermal radiation. Paris Symposium in Radio Astronomy, Ed. R.N. Bracewell, Stanford Univ. Press, p. 53-55.

Thieman, J.R.; and Goldstein, M.L. 1981. Arcs in Saturn's radio spectra. Nature 292: 728-731.

Uman, M.A. 1969. Lightning (New York: McGraw-Hill).

Warwick, J.W.; Evans, D.R.; Romig, J.H.; Alexander, J.K.; Desch, M.D.; Kaiser, M.L.; Aubier, M.; Leblanc, Y.; Lecacheux, A.; and Pedersen, B.M. 1982. Planetary radio astronomy observations from Voyager 2 near Saturn. Science 215: 582-587.

Warwick, J.W.; Pearce, J.B.; Evans, D.R.; Carr, T.D.; Schauble, J.J.; Alexander, J.K.; Kaiser, M.L.; Desch, M.D.; Pedersen, B.M.; Lecacheux, A.; Daigne, G.; Boischot, A.; and Barrow, C.W. 1981. Planetary radio astronomy observations from Voyager 1 near Saturn. Science 212: 239-243.

Warwick, J.W.; Pearce, J.B.; Peltzer, R.G.; and Riddle, A.C. 1977. Planetary radio astronomy instrument for the Voyager missions. Space Sci. Rev. 21: 309-319.

Warwick, J.W.; Pearce, J.B.; Riddle, A.C.; Alexander, J.K.; Desch, M.D.; Kaiser, M.L.; Thieman, J.R.; Carr, T.D.; Boischot, A.; Harvey, C.C; and Pedersen, B.M. 1979. Voyager 1 planetary radio astronomy observations near Jupiter. Science 204: 995-998.

Wu, C.S.; and Lee, L.C. 1979. A theory of terrestrial kilometric radiation. Astrophys. J. 230: 621-626.

Zarka, P.; and Pedersen, B.M. 1983. Statistical study of Saturn electrostatic discharges. J. Geophys. Res., in press.

FIGURE CAPTIONS

Figure 1. The trajectories of Voyager-1 and Voyager-2 projected onto the disk of Saturn. The sub spacecraft tracks remain nearly fixed in Saturn latitude and local time during the long inbound and outbound portions of the trajectories. Only during the few hours near the two closest approaches do the sub spacecraft tracks show significant motion in this coordinate system.

Figure 2. (from Kaiser et al., 1980) Simultaneous 24 hour dynamic spectra from Voyager-1 and Voyager-2. The bottom panel of each set indicates total power, with increasing darkness proportional to increasing intensity. The top panel of each pair shows the sense of polarization with RH coded as white, LH coded as black. The indicated Saturn event occurs earlier and is more intense on the Voyager-1 spectra.

Figure 3. A 24 hour total power dynamic spectra from Voyager-1 outbound at a distance of ~100 R_S. Considerable fine structure can be seen superimposed on the two major emission episodes. The vertical streaks between 12 and 24 hr are Type III solar bursts.

Figure 4. (from Warwick et al., 1981) (a) Occurrence probability of SKR at 174 kHz as a function of the sub spacecraft SLS, showing both pre and post encounter distributions. (b) The same data shown in panel a, but plotted as a function of sub solar SLS.

Figure 5. (from Kaiser et al., 1981) Typical SKR flux density spectra observed 50% (box), 10% (dot) and only 1% (bar) of the time are shown for the inbound and outbound observations of Voyager-1.

Figure 6. Flux density spectra comparing a normal episode of SKR emission with a Dione modulated episode that occurred a short time earlier. The spectra have similar shapes except for the low-frequency portion which falls off much more rapidly in the Dione case.

Figure 7. (adapted from Desch, 1982) Voyager 2 data showing close dependence between the solar wind pressure at Saturn (dashed) and the level of SKR (solid) for 90 days in 1981. Vertical scales are approximate.

Figure 8. (from Desch,1982) Results of cross correlating solar wind pressure (solid) and speed (dashed) with the level of SKR for both Voyager-1 and -2.

Figure 9. (a) Compressed SKR spectrum for 58 days around Voyager-1 Saturn encounter (day 318.0). The arrows refer to the center of the integration intervals of the spectra shown on Figure 9b. (b) Intensity spectra of SKR integrated over one rotation duration, thus eliminating intensity variations on shorter time scales.

Figure 10. PRA 10 minute averaged measurements of the apparent degree of circular polarization during the 16 days centered on the Voyager-1 (upper panle) and Voyager-2 (lower panel) closest approaches (C.A.). Spacecraft rolls are indicated by dark arrows.

Figure 11. Examples of arcs in the dynamic spectrum of Saturn emission detected by the Voyager-1 spacecraft. Data from one rotation of Saturn before

(a) and after (b) closest approach. The sub Voyager-1 SLS longitude is indicated along with the begin time of each rotation. VE and VL arcs together with an episode of 'patchy pattern' are delineated.

Figure 12. (Adapted from Boischot et al.1981) Arcs observed by Voyager-1 before (upper panel) and after (lower panel) closest approach, as a function of subsolar SLS longitude. (a) Examples of arc shapes observed during several planetary rotations. (b) Histograms of the arc orientation during the same period. VE and VL arc histograms are plotted upwards and downwards, respectively.

Figure 13. (From Kurth et al., 1982a) Trapped continuum radiation at Saturn. The lower panel is a frequency-time spectrogram showing the diffuse continuum radiation spectrum between ~500 Hz and a few kHz. The spectrum in the upper panel is a 4 second average showing the low frequency cutoff near f_p and the spectral index of ~-3 at higher frequencies.

Figure 14. (Adapted from Scarf et al., 1982) Frequency-time spectrograms showing the narrowband emissions observed by Voyager-1 and -2. These emissions are thought to extend to several tens of kHz.

Figure 15. The upper panel (from Warwick et al., 1981) shows a forty minute long dynamic spectrum at the time of Voyager-1 closest approach. Both the PRA low and high bands are shown. SED are the short, vertical streaks throughtout the panel. SKR is the dark band near 500 kHz. The lower panel shows the overall occurrence of SED for the Voyager-1 encounter period as determined by a computerized detection scheme.

Figure 16. (Adapted from Zarka and Pedersen, 1983) The duration of individual SED events for both the Voyager-1 and Voyager-2 encounters. The events were cataloged by a computer algorithm which compared successive 6-sec samples at the same observing frequency and recorded those samples which were larger by 25% or more from either the preceding or following sample. The SED events are exponentially distributed with an e-folding of about 40 msec for Voyager-1. The total number of SED detected by Voyager-2 is about a factor of three lower than Voyager-1, but the e-folding is nearly the same.

Figure 17. (from Kaiser and Desch, 1982) The best estimates for the source footprints of SKR. RH emissions comes from field lines mapping to a very small area in the northern hemisphere, and the LH emission is constrained to field lines mapping to a very narrow, long band at high southern latitudes.

Figure 18. (Adapted from Scarf et al., 1982) The position of the Voyager spacecraft when narrowband emissions below 12 kHz were detected. These observations suggest a source located at small radial distances and illuminating high latitudes.

Figure 19. (Adapted from Gurnett et al., 1981b) The bottom panel is a schematic drawing of where the source of the narrowband emissions might be located. The upper panel shows the relationship between f_{UHR} and $(n+1/2)\, f_g$ harmonics. It is thought intense electrostatic waves at $f_{UHR} = (n+1/2)\, f_g$ are the source of the narrowband emissions.

Figure 20. (after Kaiser et al., 1983) Comparison of observed and predicted recurrence patterns for the five SED episodes centered on Voyager-1 closest approach. Panel (a) shows schematically the times and frequencies where SED were detected (black) and undetected (white). Before and almost up to closest approach (CA) no SED are seen below about 5 MHz. After, CA, SED are regularly observed down to and even below 500 kHz. In between the episodes, SED are virtually absent. Panels (b), (c), and (d) compare the predicted recurrence patterns for a 60°-wide atmospheric storm system, a single point source atmospheric storm, and a single point source in the rings at 1.8 R_s, respectively. The agreement between the observed and predicted start/stop times for the 60°-wide storm system (b) is clear. Note especially the coincidence between start and stop times for the episdoe centered on closest approach, which lasts about 3 hours longer than any other episode. The single storm model (c) consistently predicts shorter episodes than those observed by about 2 hours, and the ring source model (d) consistently predicts longer episodes by about 2 hours.

Figure 21. (after Kaiser et al., 1983) Voyager-1 trajectory past Saturn is shown projected into the equatorial plane. The shaded globes show the planetary aspect and SED source location as viewed by Voyager-1 at three times near closest approach. On day 317 at 1950 SCET (spacecraft event time), the source reappears on the west limb of the planet, marking the onset of the third episode in Fig. 20. At 2100 SCET (panel a), the leading edge of the source region is about 30° onto the visible face of Saturn; at 0000 SCET (b), the leading edge is about 50° from the limb and well into the night hemisphere, permitting escape of SED below 5 MHz; by 0600 SCET (c), the trailing edge of the source is near the eastern limb, close to disappearing beyond the spacecraft horizon. At 0625 SCET the episode ends as the source disappears from Voyager-1's view.

SUB-VOYAGER TRACKS ON SATURN

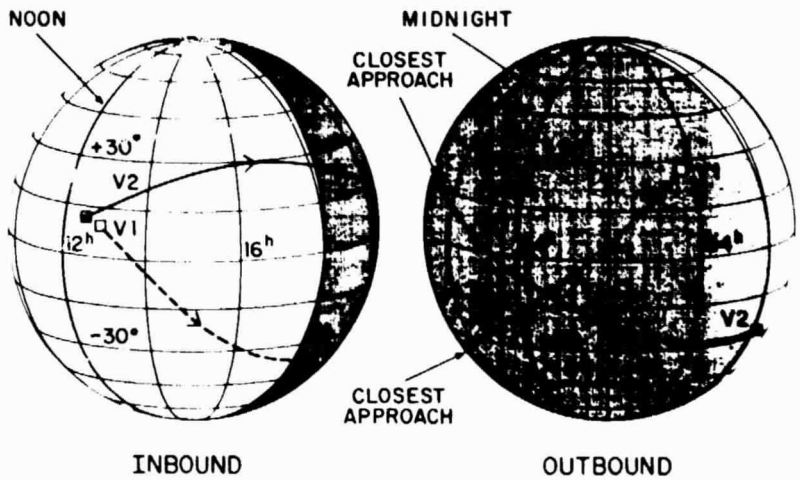

Figure 1

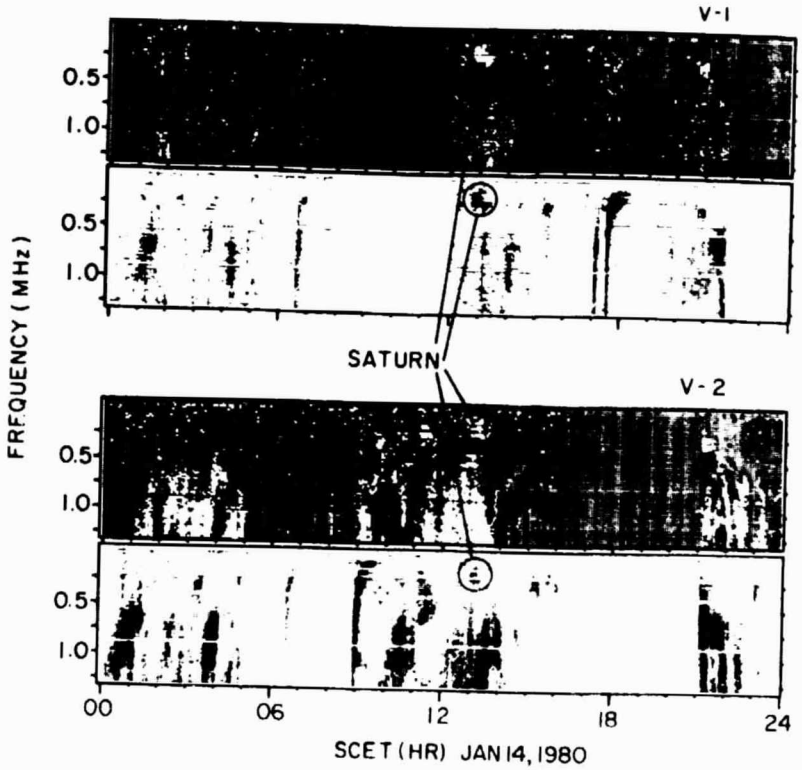

Figure 2

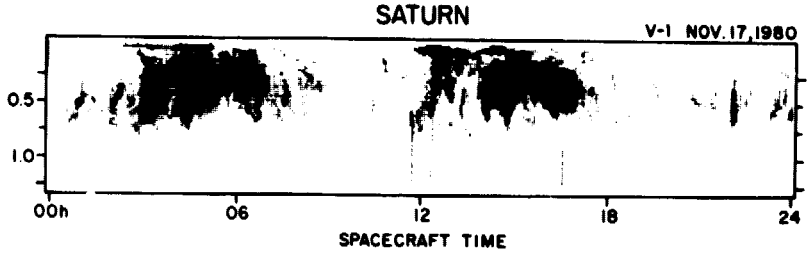

Figure 3

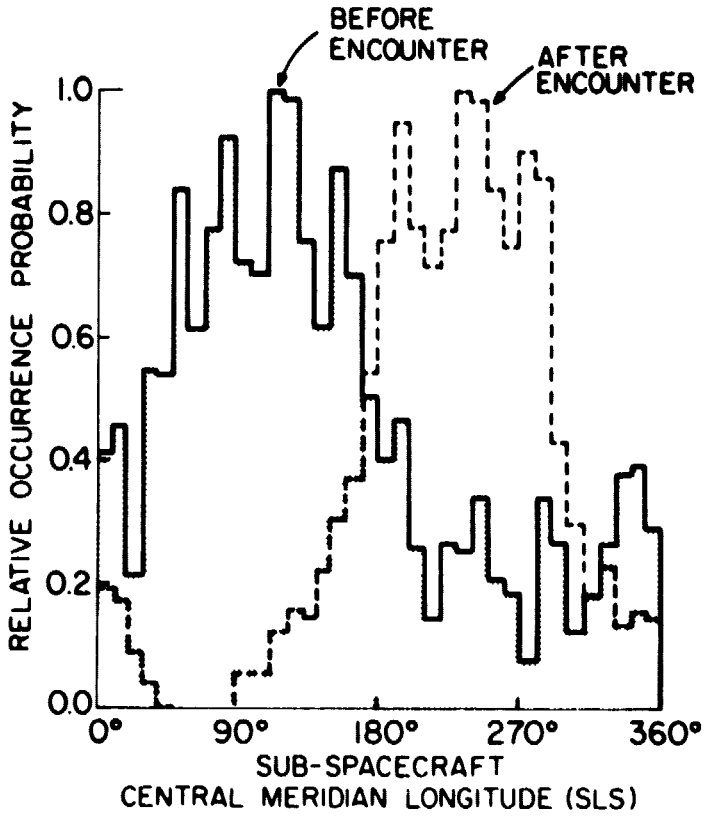

(a)

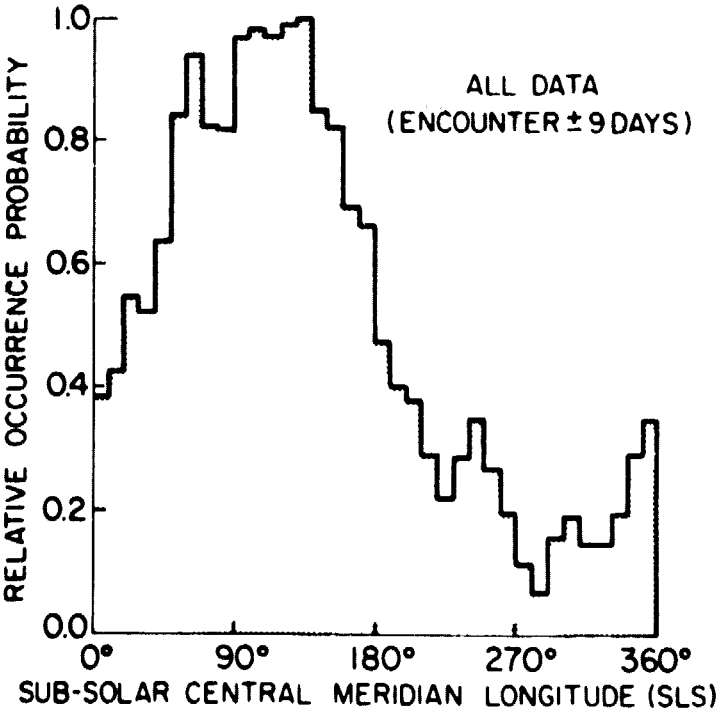

(b)

Figure 4

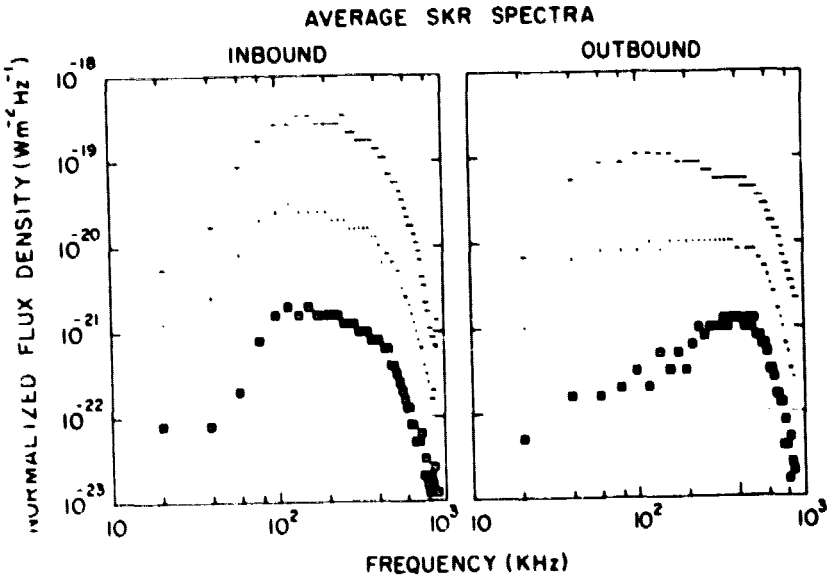

Figure 5

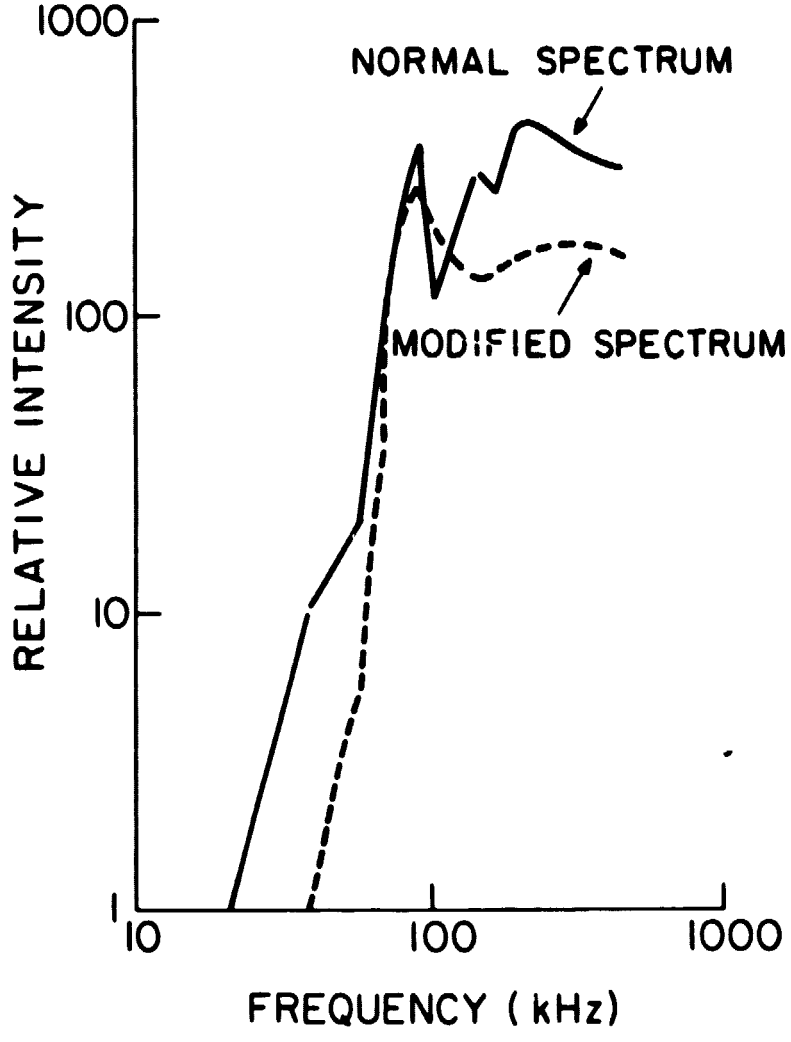

Figure 6

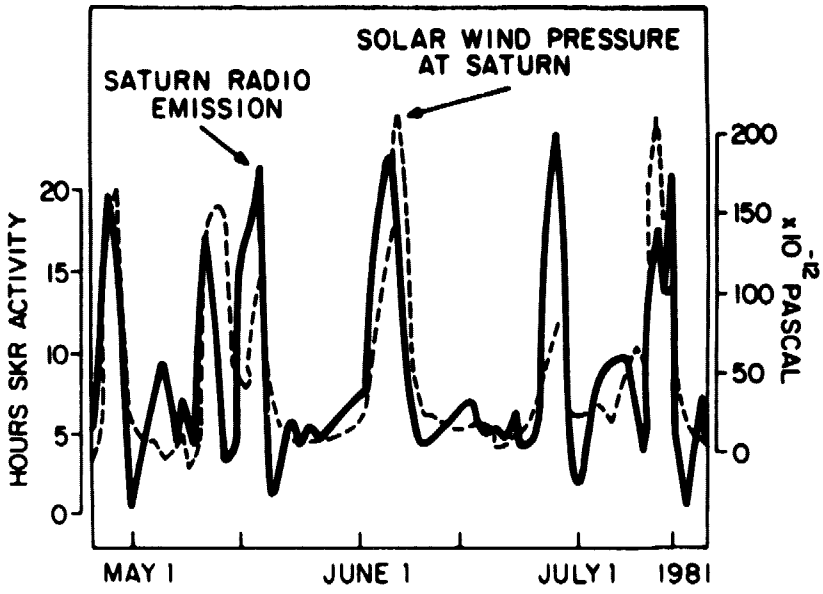

Figure 7

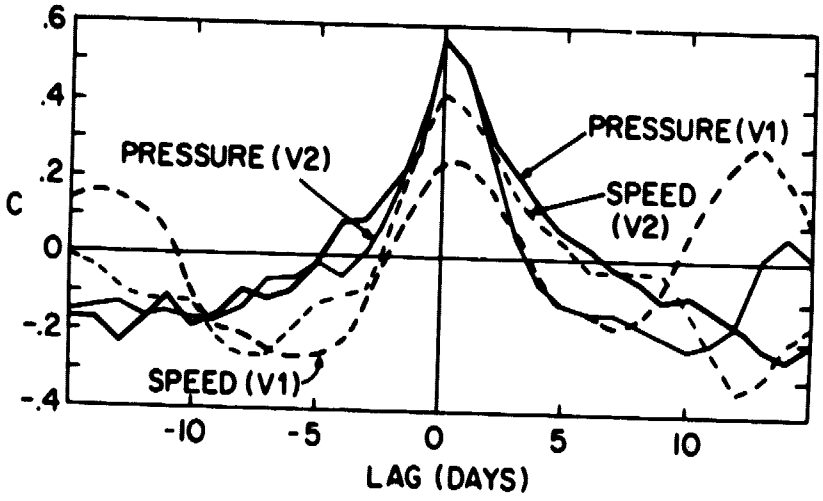

Figure 8

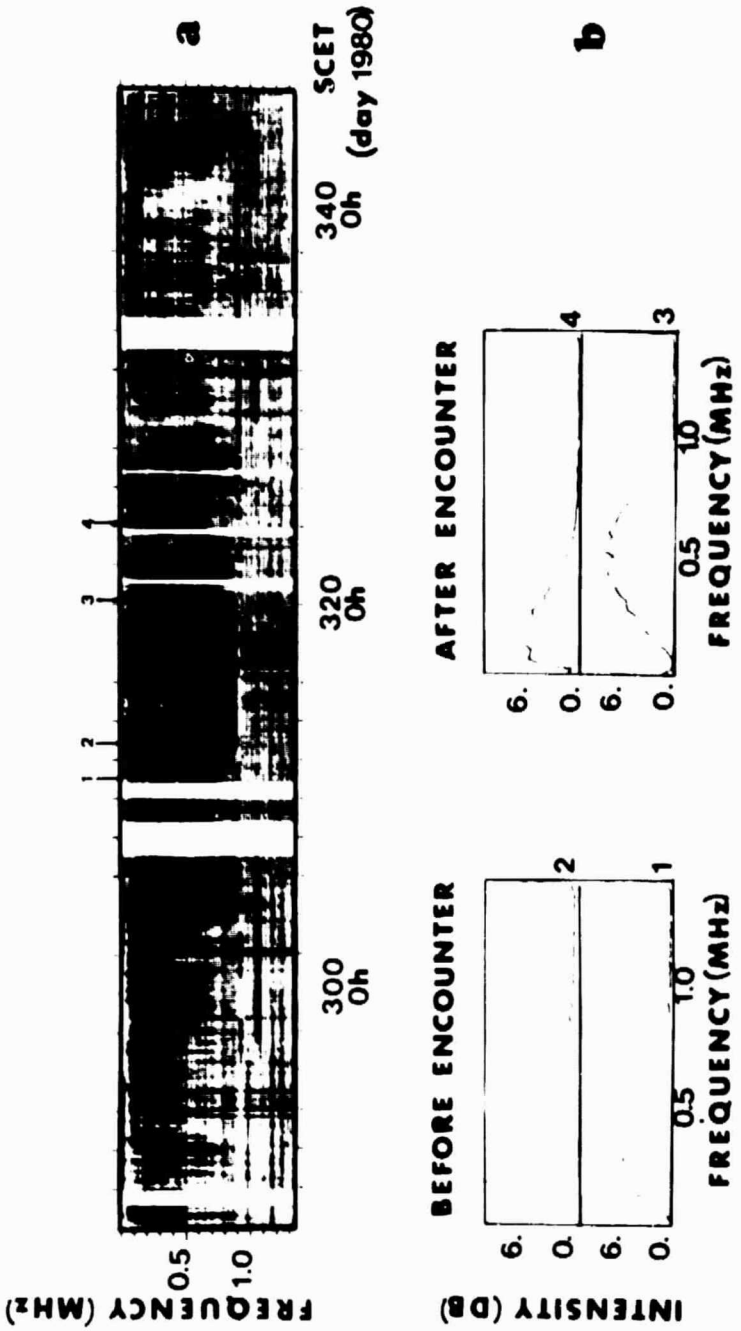

Figure 9

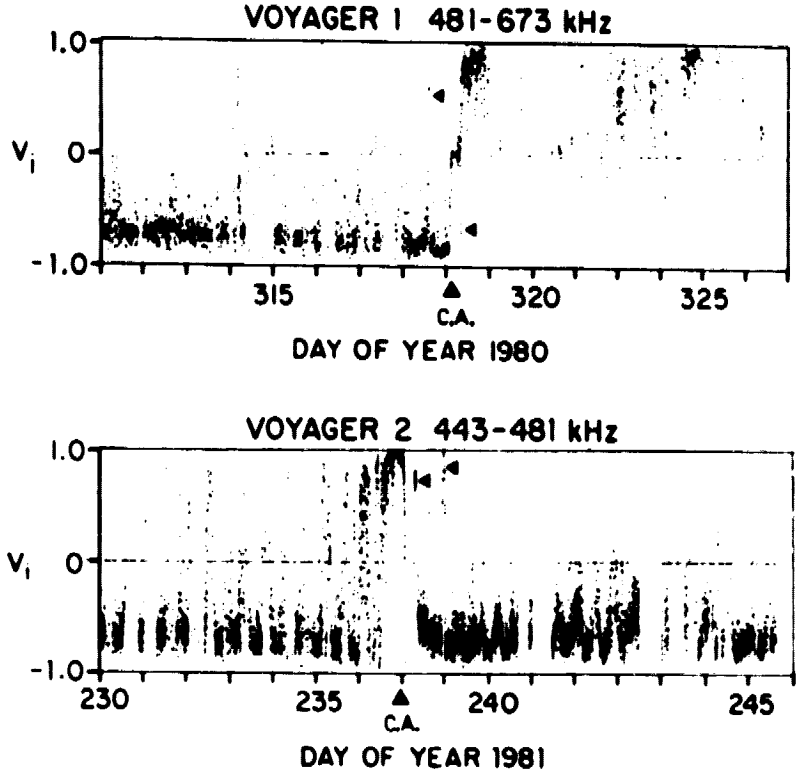

Figure 10

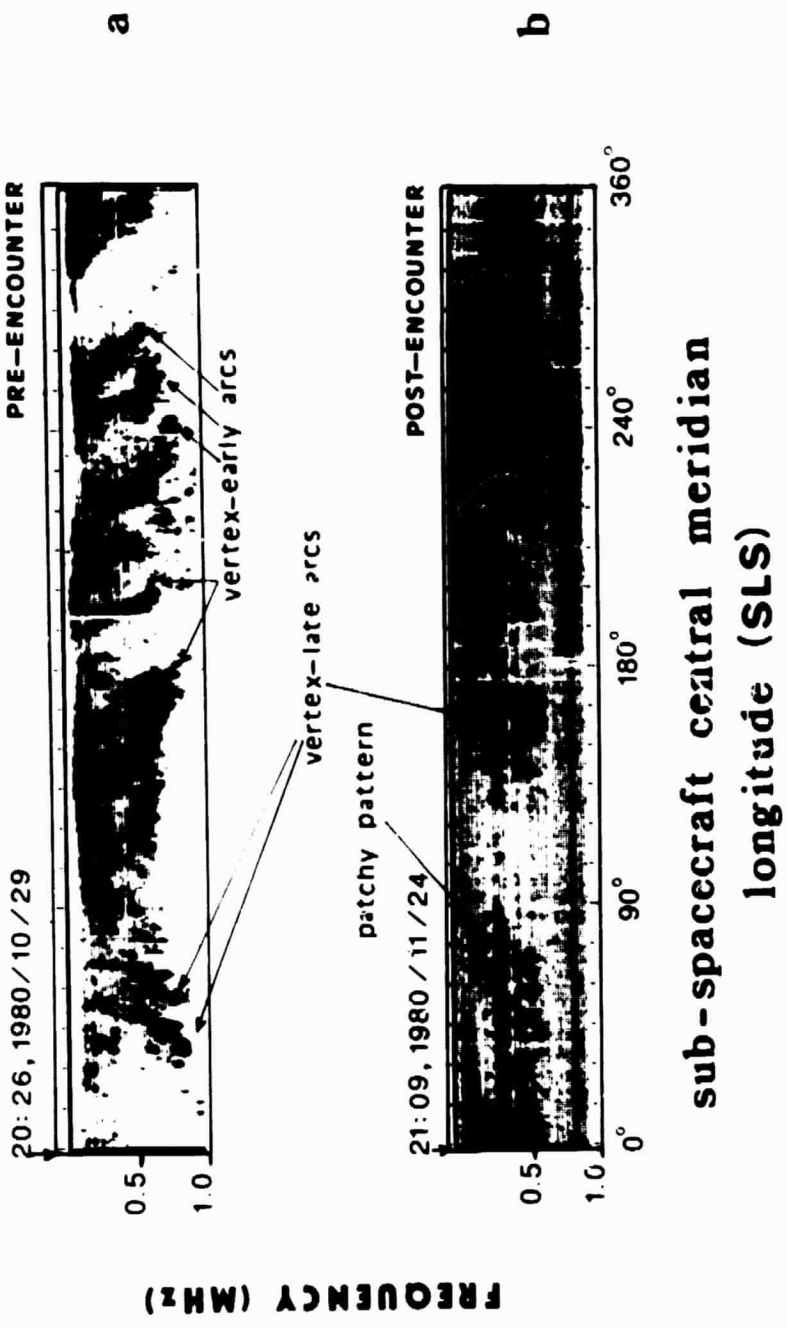

Figure 11

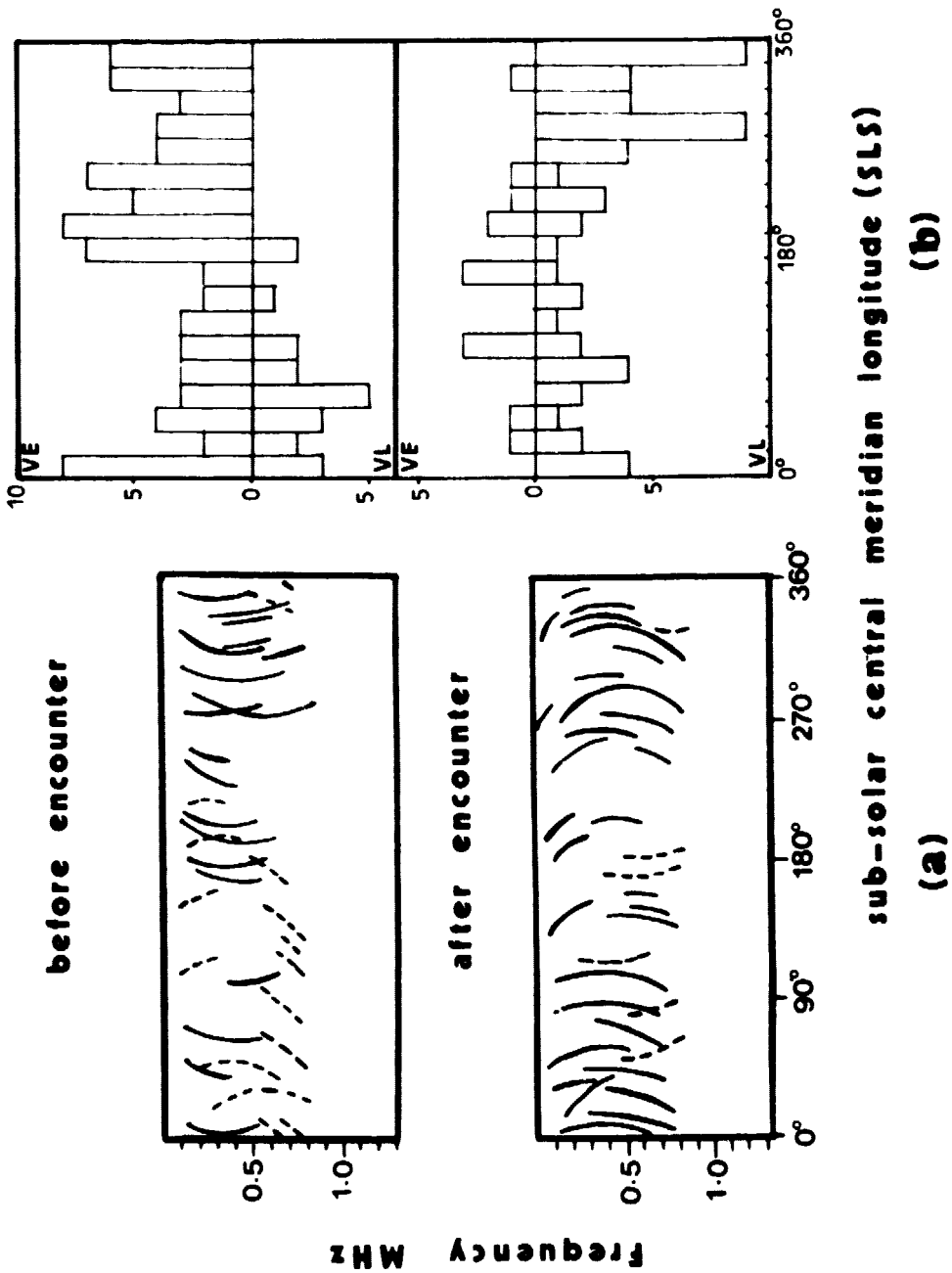

Figure 12

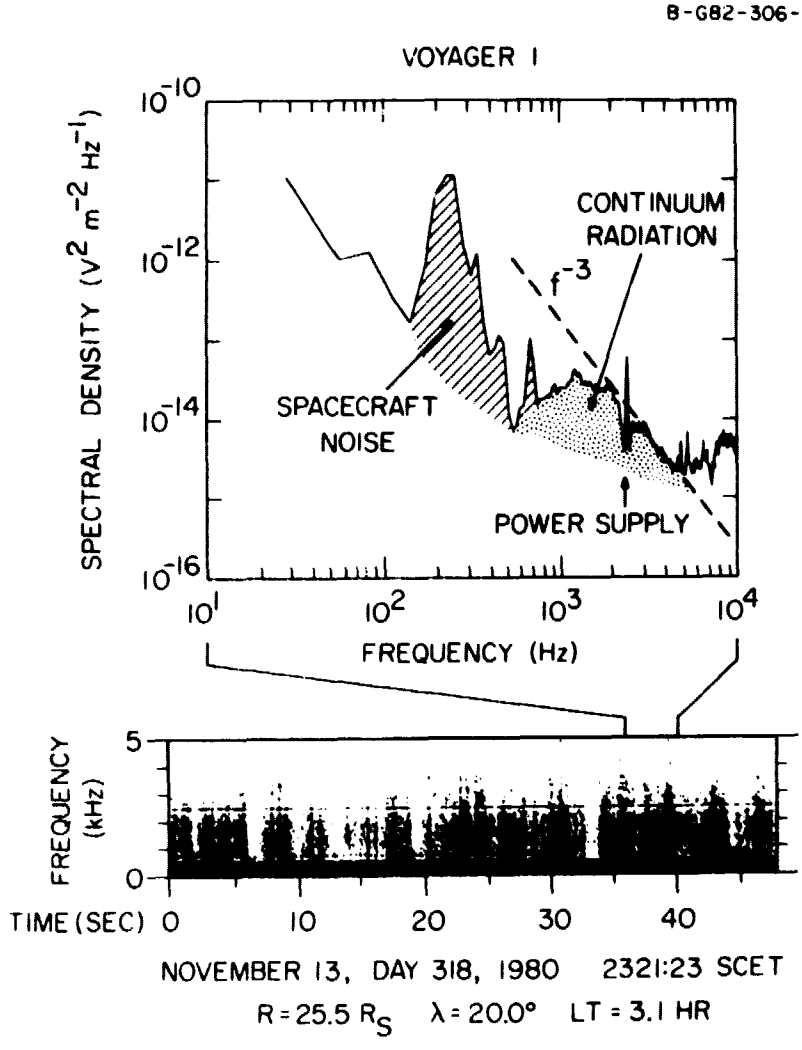

Figure 13

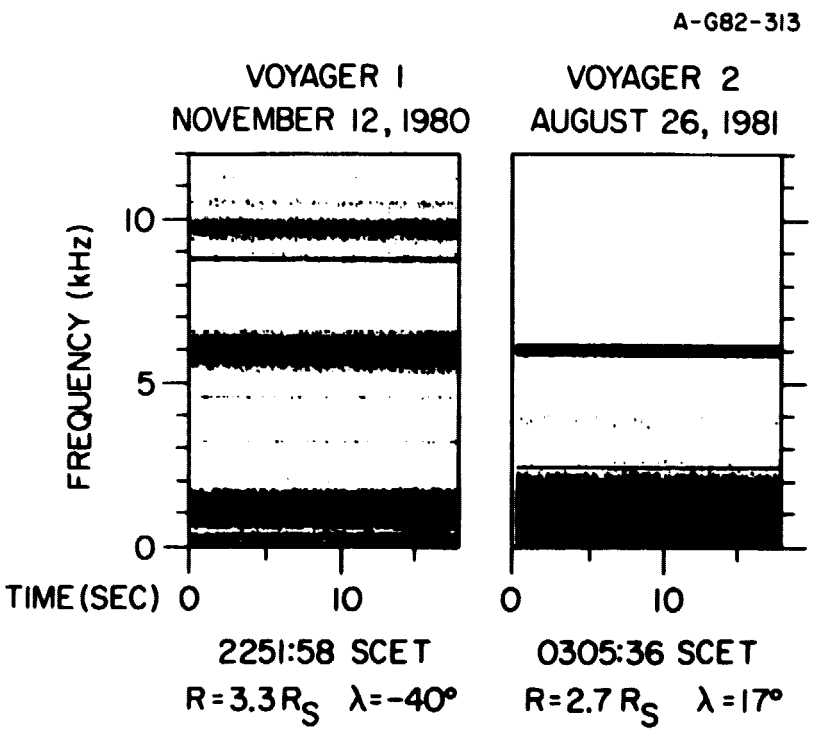

Figure 14

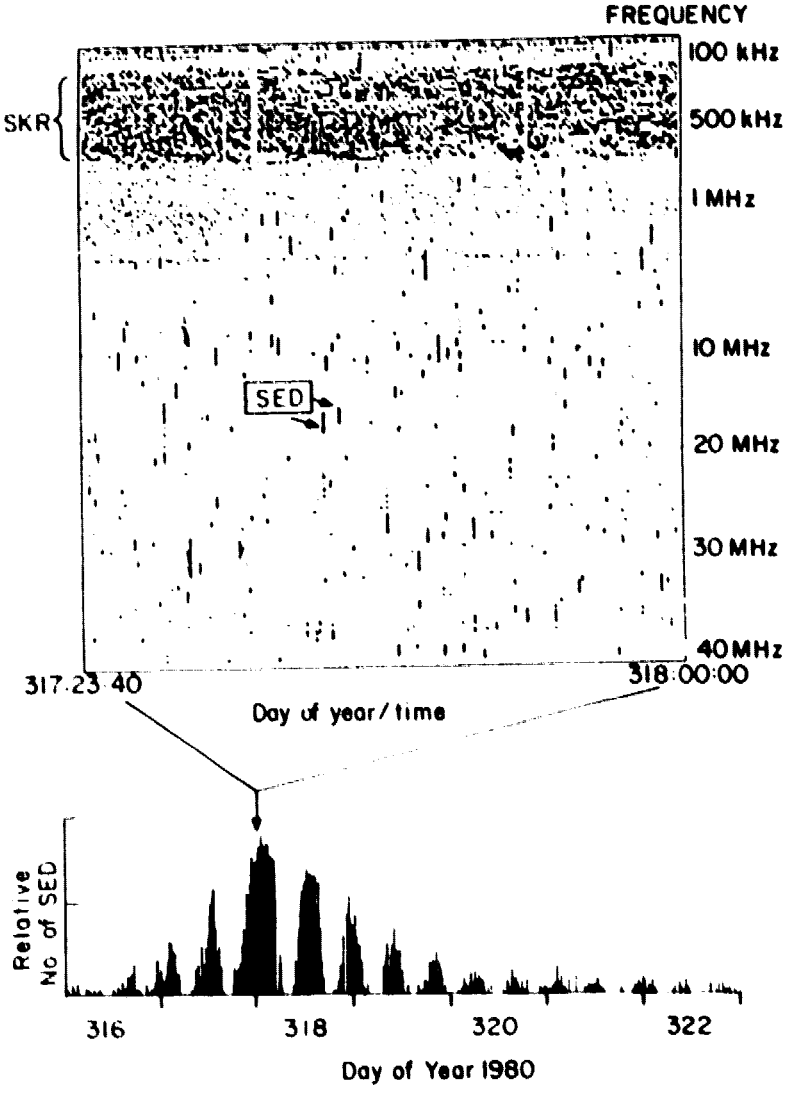

Figure 15

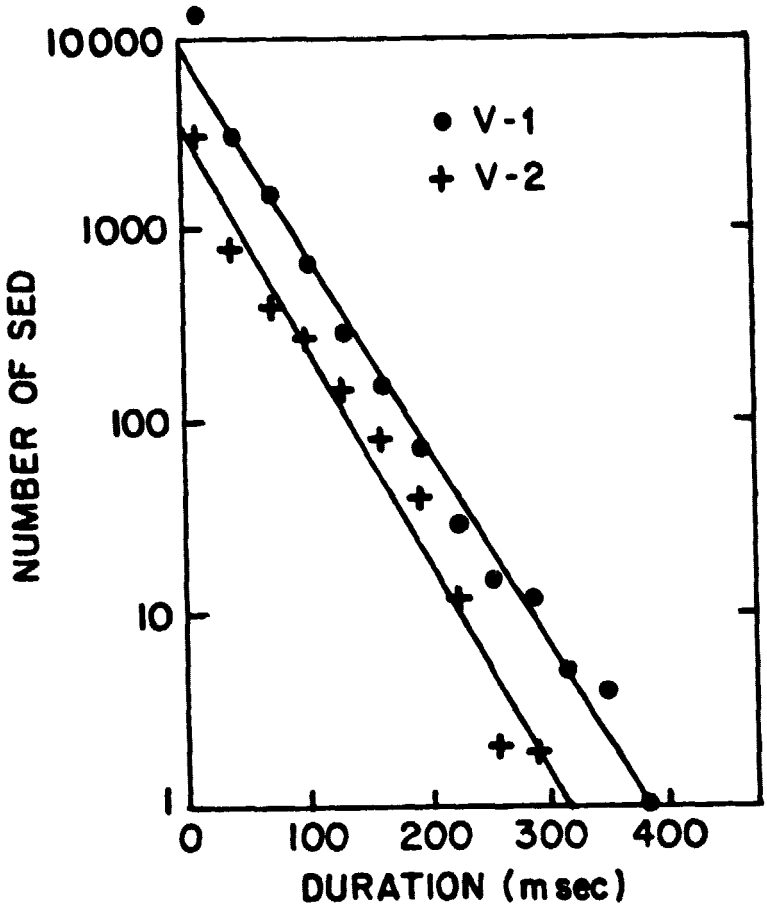

Figure 16

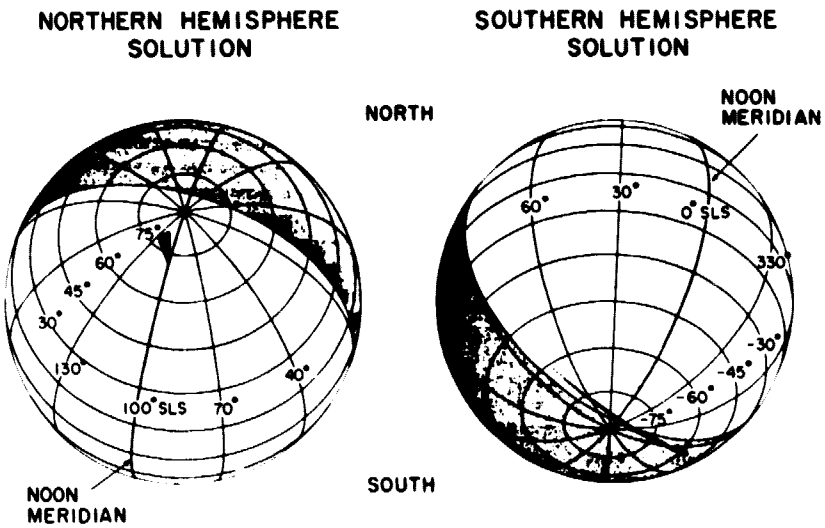

Figure 17

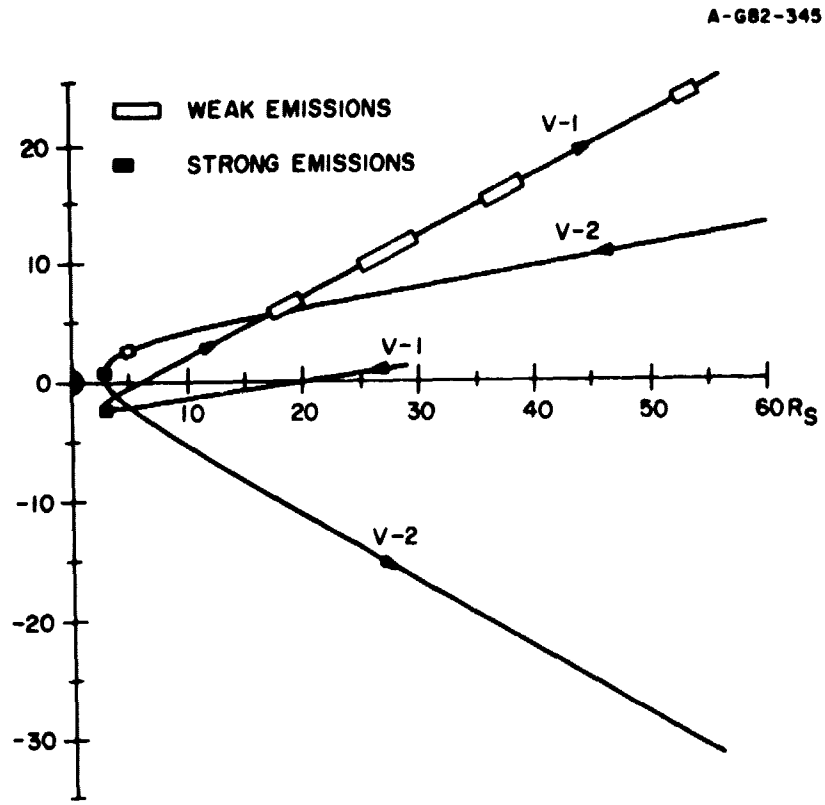

Figure 18

B-G80-872-2

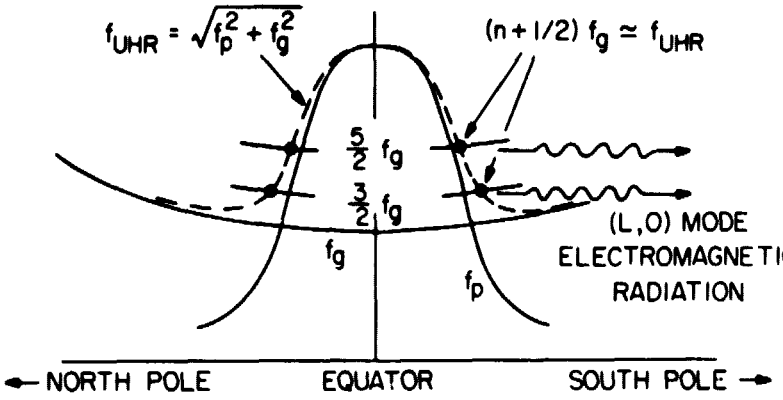

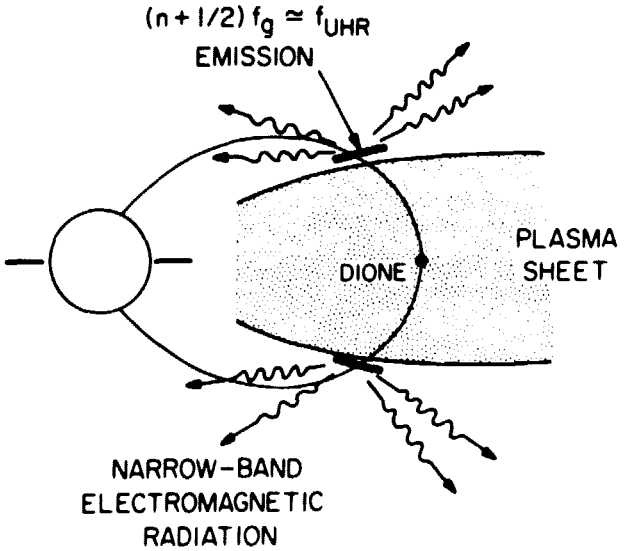

Figure 19

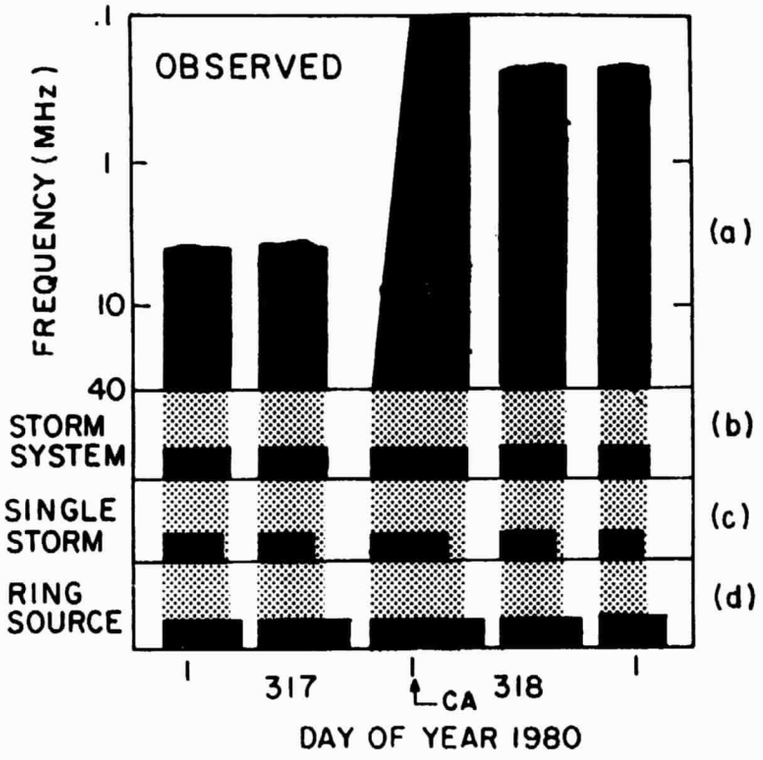

Figure 20

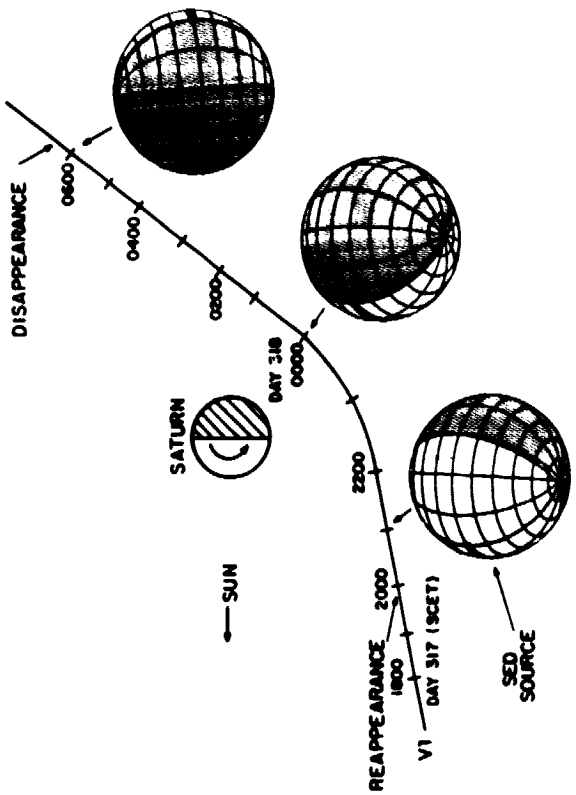

Figure 21